Gondwana Research 48 (2017) 86–100

Contents lists available at ScienceDirect

Gondwana Research

journal homepage: www.elsevier.com/locate/gr

Paleomagnetism of the Upper Cretaceous red-beds from the eastern edge of the Lhasa Terrane: New constraints on the onset of the India-Eurasia collision and latitudinal crustal shortening in southern Eurasia

Yabo Tong [a,b], Zhenyu Yang [c,*], Junling Pei [a,b], Heng Wang [d], Yinchao Xu [a], Zongwen Pu [a]

[a] Institute of Geomechanics, Chinese Academy of Geological Sciences, Beijing 100081, China
[b] Key Laboratory of Paleomagnetism and Tectonic Reconstruction, The Ministry of Land and Resources, Beijing 100081, China
[c] College of Resources, Environment and Tourism, Capital Normal University, Beijing 100048, China
[d] Institute of Geology, China Earthquake Administration, Beijing 100029, China

ARTICLE INFO

Article history:
Received 9 October 2016
Received in revised form 9 April 2017
Accepted 24 April 2017
Available online 27 April 2017

Handling Editor: J.G. Meert

Keywords:
Upper Cretaceous
Inclination shallowing
Lhasa Terrane
Paleomagnetism
India-Eurasia collision

ABSTRACT

The Late Cretaceous location of the Lhasa Terrane is important for constraining the onset of India-Eurasia collision. However, the Late Cretaceous paleolatitude of the Lhasa Terrane is controversial. A primary magnetic component was isolated between 580 °C and 695 °C from Upper Cretaceous Jingzhushan Formation red-beds in the Dingqing area, in the northeastern edge of the Lhasa Terrane, Tibetan Plateau. The tilt-corrected site-mean direction is $D_s/I_s = 0.9°/24.3°$, $k = 46.8$, $\alpha_{95} = 5.6°$, corresponding to a pole of *Plat./Plon.* = 71.4°/273.1°, with $A_{95} = 5.2°$. The anisotropy-based inclination shallowing test of Hodych and Buchan (1994) demonstrates that inclination bias is not present in the Jingzhushan Formation. The Cretaceous and Paleogene poles of the Lhasa Terrane were filtered strictly based on the inclination shallowing test of red-beds and potential remagnetization of volcanic rocks. The summarized poles show that the Lhasa Terrane was situated at a paleolatitude of 13.2° ± 8.6°N in the Early Cretaceous, 10.8° ± 6.7°N in the Late Cretaceous and 15.2° ± 5.0°N in the Paleogene (reference point: 29.0°N, 87.5°E). The Late Cretaceous paleolatitude of the Lhasa Terrane (10.8° ± 6.7°N) represented the southern margin of Eurasia prior to the collision of India-Eurasia. Comparisons with the Late Cretaceous to Paleogene poles of the Tethyan Himalaya, and the 60 Ma reference pole of East Asia indicate that the initial collision of India-Eurasia occurred at the paleolatitude of 10.8° ± 6.7°N, since 60.5 ± 1.5 Ma (reference point: 29.0°N, 87.5°E), and subsequently ~1300 ± 910 km post-collision latitudinal crustal convergence occurred across the Tibet. The vast majority of post-collision crustal convergence was accommodated by the Cenozoic folding and thrust faulting across south Eurasia.

1. Introduction

The collision of the Indian plate and Eurasia in the Paleogene is one of the most important tectonic events of the Cenozoic (Jaeger et al., 1989; Beck et al., 1995; Yin and Harrison, 2000; Aitchison et al., 2007). The subsequent continuous northward penetration of India into Asia not only induced intensive crustal tectonic deformation within south Eurasia and uplifted the Tibetan Plateau, but it also formed large-scale faults systems in the internal and surrounding area of the Tibetan Plateau. The Lhasa Terrane split from the Gondwana super-continent in the Middle-Late Triassic (Metcalfe, 2009; Zhu et al., 2011), and accreted onto the Qiangtang Terrane along the Bangong-Nujiang Suture in the Late Jurassic-Early Cretaceous (Kapp et al., 2003, 2007; Guynn et al., 2006; Qiangba et al., 2009; Zhu et al., 2013). The Lhasa Terrane formed the southern margin of Eurasia before the collision of the Indian plate and Eurasia, and thus, Cretaceous and Paleogene paleomagnetic data for the Lhasa Terrane is very important for constraining the collision time and for understanding the collision process of the Indian plate and Eurasia.

In the last three decades, although, many geological and paleomagnetic studies have been carried out in the Lhasa Terrane in order to constrain the collision process of the Indian plate and Eurasia, the subject remains controversial. For example, estimates of the collision time of the Indian plate and Eurasia range from 70 to 34 Ma (Yin and Harrison, 2000; Aitchison et al., 2007; Tan et al., 2010; Cai et al., 2011; Huang et al., 2013; Ma et al., 2014; Li et al., 2017); and estimates of post-collision latitudinal crustal convergence in the south Eurasia range from more than 1300 km (Sun et al., 2010; Ma et al., 2014; Yang et al., 2014; Li et al., 2017) to only ~200 km (Tan et al., 2010; Huang et al., 2013). These controversies arise because of the divergence of Cretaceous and Paleogene paleomagnetic data obtained from red-

* Corresponding author.
E-mail address: zhenyu.yang@cnu.edu.cn (Z. Yang).

http://dx.doi.org/10.1016/j.gr.2017.04.018
1342-937X/

beds and volcanic rocks in the Lhasa Terrane. Several reasons may be responsible for this divergence: (a) depositional and/or compaction-induced inclination shallowing of the red-beds (Tan et al., 2003; Tauxe and Kent, 2004; Gilder et al., 2008; Huang et al., 2013); (b) remagnetization of Cretaceous and Paleogene volcanic rocks (Huang et al., 2015); and (c) the secular variation of the geomagnetic field was not averaged out for the Cretaceous and Paleogene volcanic rocks (Sun et al., 2010; Yi et al., 2011; Ma et al., 2014). Although recent paleomagnetic studies have applied inclination shallowing correction and secular variation tests to the paleomagnetic data from red-beds and volcanic rocks, respectively, there are still discrepancies between the paleomagnetic data (Huang et al., 2013; Ma et al., 2014; Yang et al., 2014, 2015; Li et al., 2017). Furthermore, previous paleomagnetic studies were carried out in the central and western part of the Lhasa Terrane (Fig. 1A), and almost no paleomagnetic data were obtained from the eastern part of Lhasa Terrane until now, which also affects the accuracy of paleogeographical reconstruction of the southern margin of Eurasia prior to the India-Eurasia collision.

In the present project, we carried out new paleomagnetic analyses and an inclination shallowing test of the Upper Cretaceous red-beds in the eastern part of the Lhasa Terrane, with the aim of addressing the problem of lack of Upper Cretaceous paleomagnetic data from the eastern part of the Lhasa Terrane. Furthermore, in addition to the commonly used criteria for assessing paleomagnetic data of Vand der Voo (1990) in previous paleomagnetic studies (Chen et al., 2012; Ma et al., 2014; Yang et al., 2014; Li et al., 2017), the reliability of the inclination shallowing correction of red-beds and the possible remagnetization of volcanic rocks indicated by the magnetic carriers of the HTC were also used as criteria in order to assess the previously published Cretaceous and Paleogene paleomagnetic data from the Lhasa Terrane. Finally, the Cretaceous to Paleogene paleolatitude of the Lhasa Terrane, the timing of the initial collision of India and Eurasia and the post-collision crustal convergence in south Eurasia are discussed on the basis of our new paleomagnetic data and previously published reliable paleomagnetic data for Lhasa Terrane.

2. Regional geology and sampling

The sampling section (31°16′N, 95°53′E) is located in the Dingqing area, which is situated at the northeastern edge of the Lhasa Terrane. The Bangong-Nujiang ophiolitic melange zone extends roughly in the SEE direction, and exposures along the northern margin of the Lhasa Terrane (Zhu et al., 2013) (Fig. 1A). Lower-Middle Jurassic, Upper Cretaceous and Eocene sedimentary strata are widely distributed in the northeastern part of the Dingqiang area. The Lower-Middle Jurassic strata are named the Xihu Formation, which is mainly composed of silty argillaceous, metaquartzite, quartz sandstone and interbedded with killas, and can be divided into three segments. The Upper Jurassic Lagongtang Formation and the Lower Cretaceous Duoni Formation are absent in the Dingqing area (Fig. 1B, C). The Upper Cretaceous strata can be divided into two formations. The lower part of the Upper Cretaceous strata is named the Jingzhushan Formation, which is ~500–900 m thick in total and mainly composed of red sandstone and siltstone (Fig. 2). The Jingzhushan Formation unconformably overlies the Upper Triassic and Carboniferous-Permian limestone strata directly (Fig. 2). SE-trending thrust faults comprise the boundary between the Upper Cretaceous Jingzhushan Formation and the Upper Triassic and Carboniferous-Permian limestone strata (Fig. 1B). Abundant fossil bivalves (*Trigonioides (T.) sinensis, T. (Diversitrigonioides) bangongcoensis, T. (D.) xizangensis*) and orbitolina fossils (*Orbitolina concave*) in the Jiangzhushan Formation indicate a Late Cretaceous age (BGMRX, 1993). The upper part of the Upper Cretaceous strata is named the Bada Formation, which conformably overlies the Jingzhushan Formation and is mainly composed of coarse sandstone and conglomerate. The Paleocene strata are absent in the Dingqing area, and the Eocene Zongbai Formation unconformably overlies the Upper Cretaceous Bada Formation directly (Fig. 1B).

A total of 18 sites (~222 samples) were sampled from fine-grained sandstone and siltstones of the Upper Cretaceous Jingzhushan Formation (Fig. 2). The strata of DQ1–DQ13 sampling sites consistently tilt to the N-NW direction with low bedding dips (Fig. 1B). The strata of DQ14–DQ16 sampling sites tilt to the similar direction with that of DQ1–DQ13, but

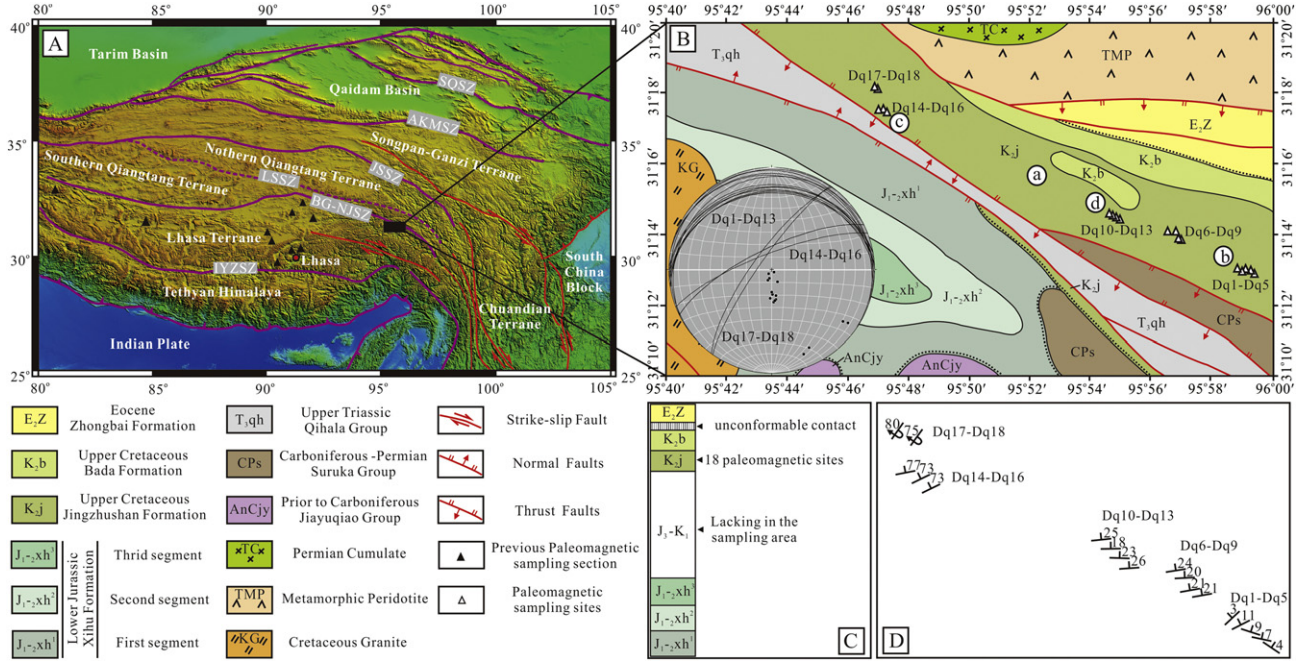

Fig. 1. (A): A schematic tectonic geological map of the Tibetan Plateau. (B): Tectonic map of the paleomagnetic sampling section of the Dingqing area and the projection of the measured bedding poles for sampling section. (C): Strike and dip of strata for each sampling site. (D): The brief chart of stratigraphic column and stratigraphic contact relationship of the Cretaceous and the Paleogene strata in the Dingqing area. The a, b, c and d in the Panel B mean a photograph has been acquired in this position, and it was shown in Fig. 2. IYZSZ, Indus-Yarlung Zangbo Suture Zone. BG-NJSZ, Bangong-Nujiang Suture Zone. LSSZ, Longmu Tso-Shuanghu Suture Zone. JSSZ, Jinshajiang Suture Zone. AKMSZ, Ayimaqing-Kunlun-Muztagh Suture Zone. SQSZ, South Qilian Suture Zone.

Fig. 2. Photographs show the Upper Cretaceous Jingzhushan red-beds in the Dingqing area. The position of photographs was marked in Fig. 1 B using a, b, c and d. (For interpretation of the references to color in this figure legend, the reader is referred to the web version of this article.)

with steep bedding dips. The DQ17 and DQ18 sampling sites were sampled close to the DQ14–DQ16 sampling sites, however, the strata of DQ17 and DQ18 sampling sites tilt to the ES direction with very high bedding dips. The field observations show that the sampling strata of the DQ14–DQ17 is relative continuous, and fold hinge zone is not located between the DQ16 and DQ17 sampling sites, indicating the DQ17 and DQ18 sampling sites experienced overturning (Fig. 1D). In order to test the possibility of depositional and/or compaction-induced inclination shallowing of the Upper Cretaceous red-beds, a total of 5 hand specimens oriented on the strata bedding were sampled from five sampling sites (DQS1 for the DQ1 site, DQS3 for the DQ3 site, DQS6 for the DQ6 site, DQS9 for the DQ9 site, DQS11 for the DQ11 site). All samples were collected with a portable drill and oriented with a magnetic compass. The location of each sampling site was determined using a portable GPS. The present geomagnetic field direction of the sampling section was calculated using the International Geomagnetic Reference Field (2010) (International Association of Geomagnetism and Aeronomy, 2010). All core samples were cut into standard specimens with a length of 2.2–2.3 cm in the laboratory for rock magnetic and thermal demagnetization experiments.

3. Rock magnetic measurements and results

The progressive acquisition of isothermal remanent magnetization (IRM) was used to determine the coercivity spectrum of the magnetic minerals. In addition, thermal demagnetization of a three-component IRM (applying successively to each of the three axes with different DC field of 2.5 T for Z axis, 0.4 T for X axis, and 0.12 T for Y axis, respectively) was used to reveal the unblocking temperatures of different magnetic minerals (Lowrie, 1990). A total of six representative standard specimens (DQ1–7, DQ4–9, DQ7–10, DQ12–5, DQ16–2, and DQ18–12) were selected for rock magnetic experiments, based on the distribution of paleomagnetic sites and lithological characteristics of the samples.

The rock magnetic results for the six specimens exhibit similar magnetic behavior (Fig. 3). The IRM acquisition curves reveal that, except for DQ7–10, the remanence of the specimens increased slowly when the applied DC field was less than 200 mT. Subsequently, the remanence of all six specimens did not approach saturation when the applied DC field approached 2400 mT. During the application of the reversed DC field, the remanence of the six specimens decreased rapidly and was then reduced to zero following the application of reversed fields in the range of 400–700 mT, indicating the presence of high coercivity magnetic minerals such as goethite and/or hematite (Fig. 3A). Thermal demagnetization of three-component IRM revealed that, except for DQ12–5, the hard and medium remanence components of other five specimens decreased in the temperature interval of 80–250 °C, and meanwhile slightly inflections were found in the DQ1–7, DQ4–9, DQ7–10 and DQ16–2, indicating the possible presence of goethite (Fig. 3B). Except for DQ7–10, the hard and medium components of the other five specimens exhibited a slight decrease when the thermal demagnetization temperature reached 300–400 °C, indicating the possible occurrence of pyrrhotite. Subsequently, the hard and medium components of the six specimens were reduced and exhibited a slight inflection in the temperature interval of 520–600 °C; in addition, even the soft components of DQ1–7, DQ4–9 and DQ7–10 were reduced to zero, indicating the occurrence of magnetite (Fig. 3B). When the thermal demagnetization temperature exceeded 640 °C, the medium and hard components of all six specimens were reduced rapidly and finally unblocked at a higher temperature than 660 °C, indicating the abundance of hematite (Fig. 3B). Thus, hematite and a minor amount of magnetite are likely to be the main magnetic carriers of the Jingzhushan Formation, with a small amount of pyrrhotite and goethite also being present in some cases.

4. Paleomagnetic measurements and results

The paleomagnetic experiments were applied in the Key Laboratory of Paleomagnetism and Tectonic Reconstruction, Ministry of Land and Resources, Beijing. All standard specimens were subjected to stepwise thermal demagnetization using an ASC TD-48 thermal demagnetizer. Remanent magnetization was measured using a 2G-755 cryogenic magnetometer. The stepwise thermal demagnetization was performed up to

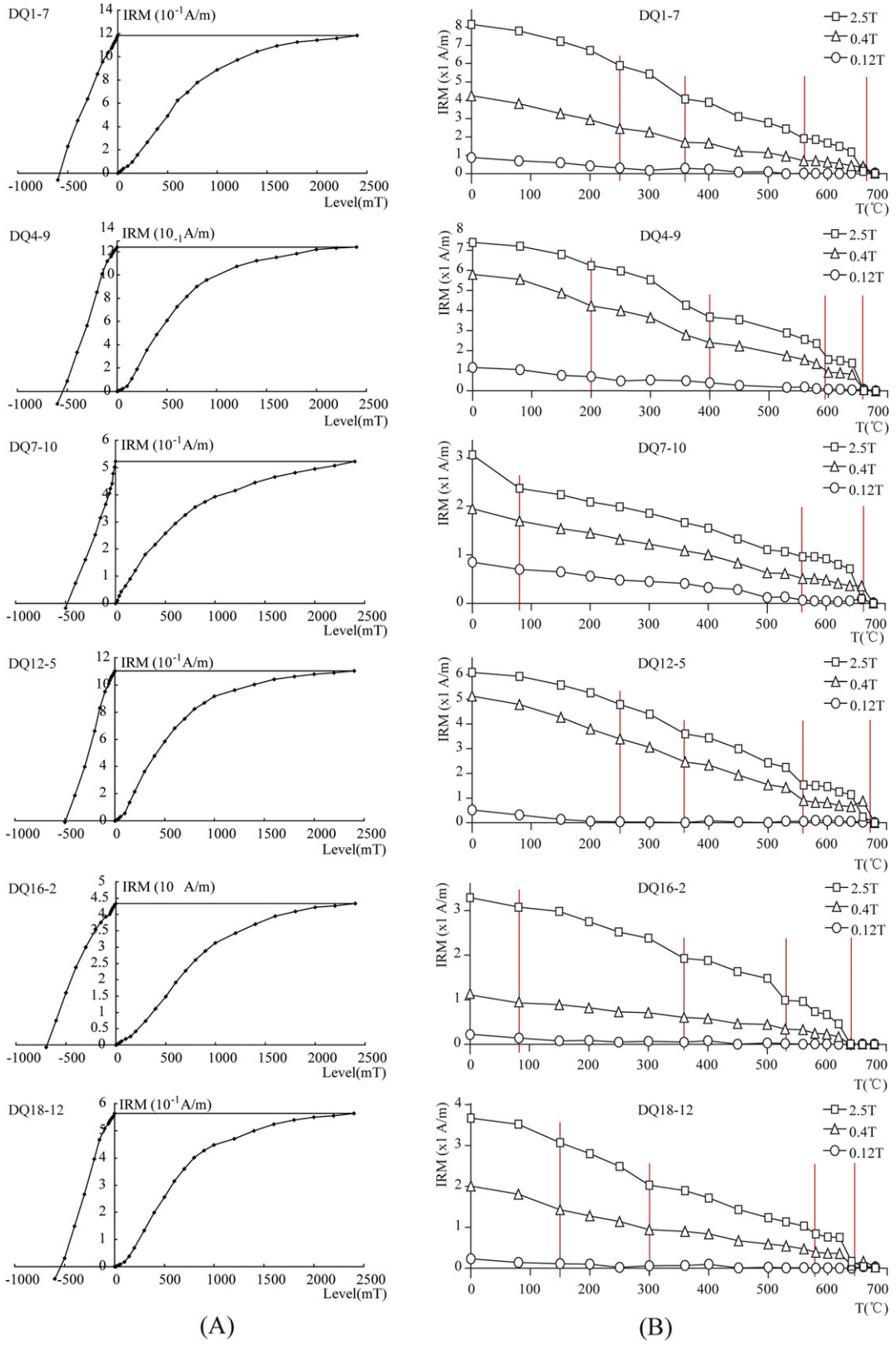

Fig. 3. The rock magnetic results of representative specimens of the Upper Cretaceous Jingzhushan Formation red-beds. (A): IRM acquisition curve and back-field demagnetization. (B): Thermal demagnetization of IRM. Thermal demagnetization of three components IRM produced by applying a different DC field (2.5 T, 0.4 T and 0.12 T) to each of three perpendicular axes of a specimen.

695 °C, according to the rock magnetic results. The temperature interval used for thermal demagnetization was 50–100 °C initially, and 10–20 °C at higher temperatures. The magnetic behavior of specimens during thermal demagnetization was plotted using a Zijderveld diagram (Zijderveld, 1967). The directions of the characteristic remanent magnetization of the specimens were determined using principal components analysis (Kirschvink, 1980). Site-mean directions were calculated using Fisher's statistics (Fisher, 1953).

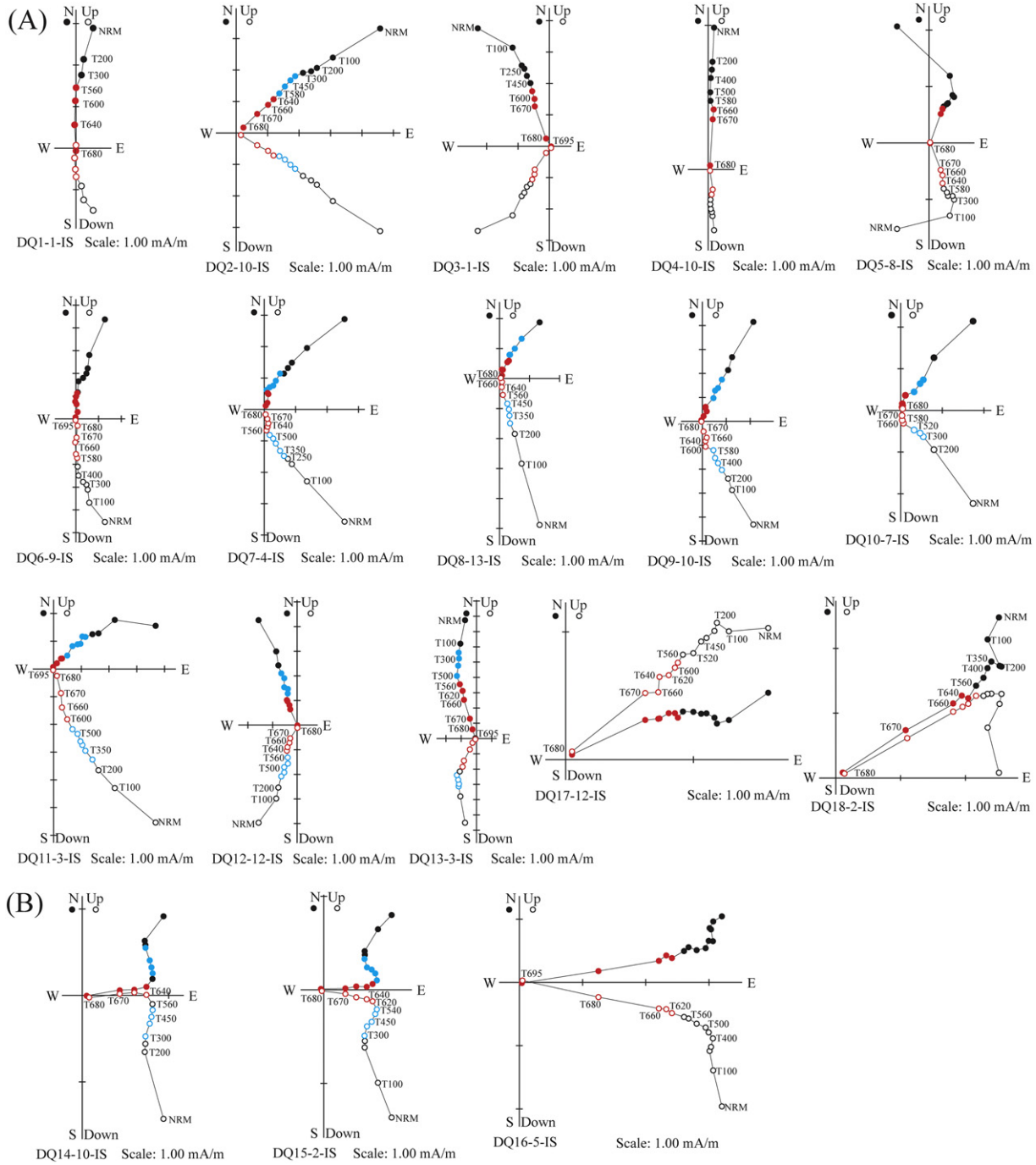

Fig. 4. Orthogonal projections of magnetization vector end-points for representative specimens of the Upper Cretaceous Jingzhushan Formation red-beds in geographic coordinates. (A): The first group consists of specimens from sites DQ1–DQ13 and DQ17–DQ18. (B): The second group consists of specimens from sites DQ14–DQ16. Solid/open symbols for horizontal/vertical projection in geographic coordinates. The blue points and red points show the thermal demagnetization temperature intervals that MTCs and HTCs being isolated, respectively. (For interpretation of the references to color in this figure legend, the reader is referred to the web version of this article.)

The low-temperature magnetic components (LTC) were isolated from 148 specimens at 18 sampling sites when the temperature reached ~300 °C (Fig. 4). Because the sample-mean direction of LTC can reflect the characteristic of LTC direction and the orientational accuracy of samples, the sample-mean direction of LTC is often used in paleomagnetic studies. The sample-mean direction of the LTC before tilt correction is $D_g = 10.4°$, $I_g = 43.4°$, $k = 19.0$, $\alpha_{95} = 2.7°$, $n = 148$ (samples), which is close to the present geomagnetic field direction (PGF) (D = 4.2°, $I = 48.9°$) and the geocentric axial dipole direction (GAD) (D = 0.0°, $I = 50.5°$) at the sampling locality. The mean direction is $D_s =$

Fig. 5. (A): Equal-area projections of the sample mean direction for LTCs before and after tilt correction. (B): Equal-area projections of the site mean direction for MTCs before and after tilt correction. (C): Equal-area projections of site-mean direction for HTCs of the first group before and after tilt correction, and progressive unfolding of the mean direction. (D): Equal-area projections of site-mean direction for HTCs of the second group before and after tilt correction. (E): Equal-area projections of site-mean direction for HTCs before and after tilt correction. Blue shaded circles around the red stars in the (A), (B), (C), (D) and (E) denote the 95% confidence limit and mean directions of sampling section. Solid and open symbols denote the lower and upper hemisphere, respectively. The red circles with blue dashed circle in the (E) are the average inclination and error of the average inclination for the sampling section. (For interpretation of the references to color in this figure legend, the reader is referred to the web version of this article.)

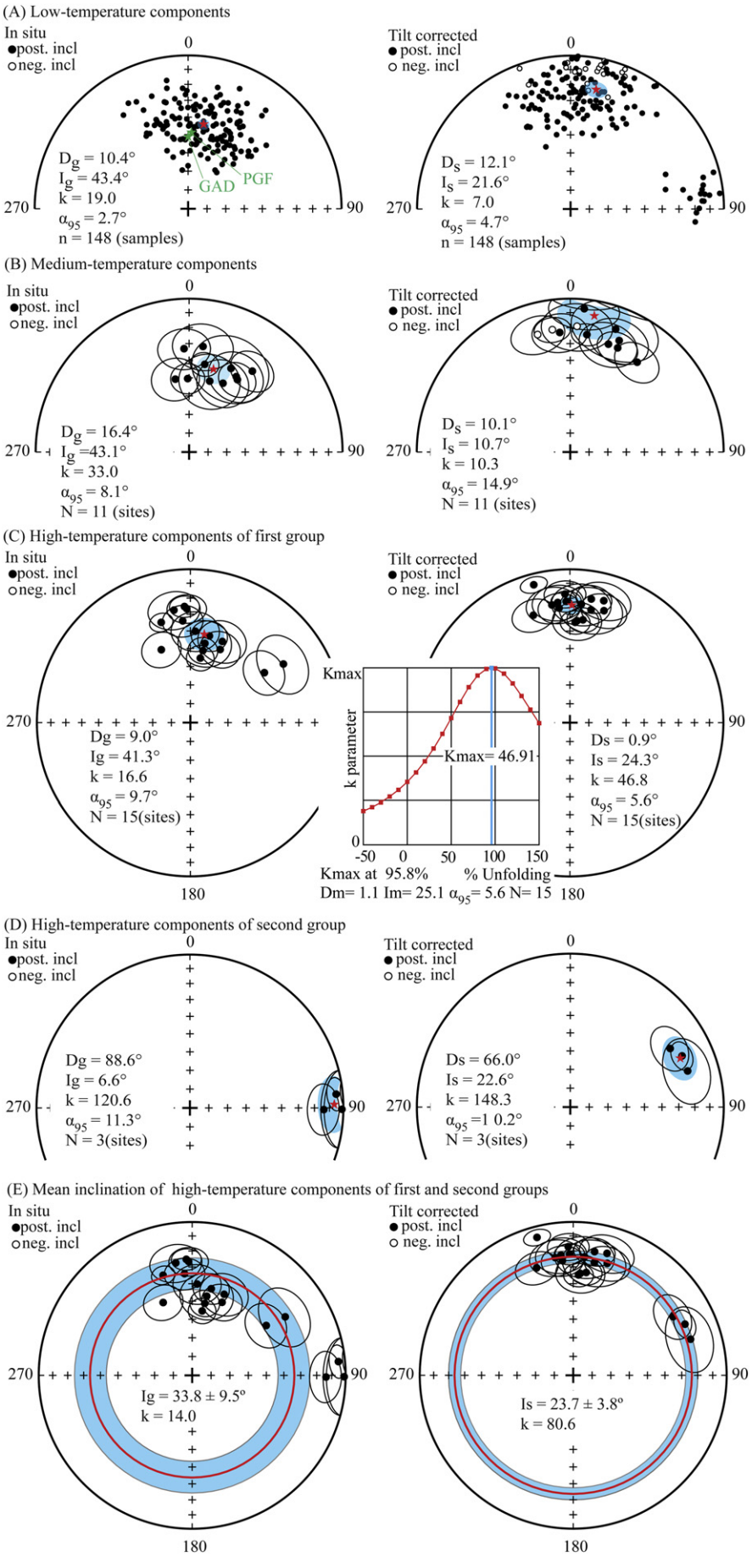
(A) Low-temperature components
In situ
●post. incl
○neg. incl
Dg = 10.4°
Ig = 43.4°
k = 19.0
α95 = 2.7°
n = 148 (samples)
GAD
PGF
Tilt corrected
● post. incl
○ neg. incl
Ds = 12.1°
Is = 21.6°
k = 7.0
α95 = 4.7°
n = 148 (samples)
(B) Medium-temperature components
In situ
●post. incl
○neg. incl
Dg = 16.4°
Ig =43.1°
k = 33.0
α95 = 8.1°
N = 11 (sites)
Tilt corrected
● post. incl
○ neg. incl
Ds = 10.1°
Is = 10.7°
k = 10.3
α95 = 14.9°
N = 11 (sites)
(C) High-temperature components of first group
In situ
●post. incl
○neg. incl
Dg = 9.0°
Ig = 41.3°
k = 16.6
α95 = 9.7°
N = 15(sites)
Kmax
k parameter
Kmax= 46.91
-50 0 50 100 150
Kmax at 95.8%
% Unfolding
Dm= 1.1 Im= 25.1 α95= 5.6 N= 15
Tilt corrected
● post. incl
○ neg. incl
Ds = 0.9°
Is = 24.3°
k = 46.8
α95 = 5.6°
N = 15(sites)
(D) High-temperature components of second group
In situ
●post. incl
○neg. incl
Dg = 88.6°
Ig = 6.6°
k = 120.6
α95 = 11.3°
N = 3(sites)
Tilt corrected
● post. incl
○ neg. incl
Ds = 66.0°
Is = 22.6°
k = 148.3
α95 =1 0.2°
N = 3(sites)
(E) Mean inclination of high-temperature components of first and second groups
In situ
●post. incl
○neg. incl
Ig = 33.8 ± 9.5°
k = 14.0
Tilt corrected
● post. incl
○ neg. incl
Is = 23.7 ± 3.8°
k = 80.6

12.1°, $I_s = 21.6°$, $k = 7.0$, $\alpha_{95} = 4.7°$ after tilt correction (Fig. 5A). The precision parameter (k) decreases from 19.0 (k_g) to 7.0 (k_s) after tilt correction, suggesting that the LTC is a viscous remanent magnetization.

The medium-temperature magnetic components (MTC) were isolated from specimens at 11 sampling sites (Table 1). Most of MTCs were isolated in the temperature interval of 300 °C–520 °C (Fig. 4). Combining with the rock magnetic result shows that the MTC is mainly carried by pyrrhotite and magnetite. The site-mean direction of the MTC is $D_g = 16.4°$, $I_g = 43.1°$, $k = 33.0$, $\alpha_{95} = 8.1°$, $N = 11$ (sampling sites) before tilt correction, and $D_s = 10.1°$, $I_s = 10.7°$, $k = 10.3$, $\alpha_{95} = 14.9°$ after tilt correction (Fig. 5B). Application of the fold test of McElhinny (1964) indicated that $k_s/k_g = 0.31 < F(20, 20) = 2.12$, and thus a negative fold test result at the 95% confidence limit. In the McFadden fold test (McFadden, 1990), the calculated values are $\xi_{(2)\text{in situ}} = 1.35$ in geographic coordinates and $\xi_{(2)\text{tilt corrected}} = 3.86$ after tilt correction, while the critical value is $\xi_C = 7.80$ at the 95% confidence limit, also indicating a negative fold test at the 95% confidence limit. Thus, the MCT should be a remagnetization component.

The high-temperature components (HTC) were isolated from specimens at all 18 sampling sites (Table 1). Most of HTCs could be isolated in the temperature interval of 540 °C–695 °C, with the unblocking temperature of 695 °C or 680 °C. A small number of HTCs were isolated in the temperature interval of 620 °C–695 °C, with the unblocking temperature of 695 °C or 680 °C. Combining with the rock magnetic result shows that the HTC of most specimens are carried by both magnetite and hematite, and for small amount of specimens, the HTC are carried by hematite alone. The HTCs can be divided into two groups based on the direction of the HTC. The first group (H1) consists of sites DQ1–DQ13 and DQ17–DQ18 (Fig. 4A). All specimens within H1 exhibit normal polarity. The site-mean direction is $D_g = 9.0°$, $I_g = 41.3°$, $k = 16.6$, $\alpha_{95} = 9.7°$, $N = 15$ (sampling sites) before tilt correction, and $D_s = 0.9°$, $I_s = 24.3°$, $k = 46.8$, $\alpha_{95} = 5.6°$ after tilt correction (Table 2, Fig. 5C). Application of the fold test of McElhinny (1964) shows that $k_s/k_g = 2.82 > F(28, 28) = 1.88$, indicating a positive fold test at the 95% confidence limit. In the McFadden fold test (McFadden, 1990), the calculated values are $\xi_{(2)\text{in situ}} = 8.25$ in geographic coordinates and $\xi_{(2)\text{tilt corrected}} = 1.06$ after tilt correction, while the critical value is $\xi_C = 4.51$ at 95% confidence limit, also indicating a positive fold test at the 95% confidence limit. In addition, the precision parameter (k) reaches a maximum ($k_{max} = 46.91$) at 95.8% unfolding during progressive unfolding (Watson and Enkin, 1993), and the direction ($D_m = 1.1°$, $I_m = 25.1°$, $k = 46.91$, $\alpha_{95} = 5.6°$) is consistent with the mean direction after tilt correction (Fig. 5C). Thus, the mean direction of H1 after tilt correction is of pre-fold origin.

The second group (H2) consists of sites DQ14–DQ16 (Fig. 4B). All of the specimens in H2 exhibit normal polarity. The site-mean direction is $D_g = 88.6°$, $I_g = 6.6°$, $k = 120.6$, $\alpha_{95} = 11.3°$, $N = 3$ (sampling sites) before tilt correction, and $D_s = 66.0°$, $I_s = 22.6°$, $k = 148.3$, $\alpha_{95} = 10.2°$ after tilt correction (Table 2, Fig. 5D). In the McFadden fold test (McFadden, 1990), the calculated values are $\xi_{(2)\text{in situ}} = 2.68$ in geographic coordinates and $\xi_{(2)\text{tilt corrected}} = 0.54$ after tilt correction, while the critical value is $\xi_C = 2.07$ at the 95% confidence limit, indicating an inconclusive fold test at the 95% confidence limit. Although the tilt corrected site-mean declination of H2 differs from that of H1, the tilt corrected site-mean inclination of H2 (22.6°) is similar to that of H1 (24.3°). The DQ14–DQ16 sampling sites are close to the thrusting fault between the Upper Cretaceous and Upper Triassic strata, which could induce local rotational deformation of DQ14–DQ16 sampling sites relative to the DQ1–DQ13 sampling sites, and result in the deviation of tilt corrected site-mean declination of H2 from the others. The groups H1 and H2 were combined to calculate the site-mean inclination using the method of maximum likelihood estimation of McFadden and Reid (1982), The inclination was 33.8° ± 9.5° with $k = 14.0$ before tilt correction and 23.7° ± 3.8° with $k = 80.6$ after tilt correction, which is consistent with that of H1 (24.3°) (Fig. 5E). The k value increased from 14.0 in situ to 80.6 after tilt correction, indicating that H2 should also have a pre-folding origin.

The paleopoles of each sampling site were calculated, and then the average Late Cretaceous paleopole of the Dingqing area was calculated using Fisher's statistic (Fisher, 1953) (Table 2). Although H2 has a pre-folding origin, it was still not used in the following discussion, because of the strong local rotations of the sampling sites. The average Late Cretaceous paleopole is 71.4°N/273.1°E for sites DQ1–DQ13 and DQ17–DQ18.

5. Reliability of the paleomagnetic data

5.1. The acquisition time of the HTCs

The Lower-Middle Jurassic, Upper Cretaceous and Eocene strata developed in the Dingqing area experienced intense folding. Since the Late Jurassic, the southern edge of Eurasia remained in a state of latitudinal compression because of the collision between the Lhasa Terrane and the Qiangtang Terrane in the Late Jurassic-Early Cretaceous (Kapp et al., 2003, 2007; Guynn et al., 2006; Qiangba et al., 2009; Zhu et al., 2013), and the subsequent collision between the Indian plate and Eurasia. The Upper Triassic strata were thrust on to the Upper Cretaceous Jingzhushan Formation on the north side and on to the Lower-Middle Jurassic Xihu Formation on the south side (Fig. 2B). Paleocene strata are absent in the Dingqing area, and the Eocene sedimentary strata unconformably overlie the Upper Cretaceous strata directly (Fig. 1B), indicating the folding of the Upper Cretaceous strata should have commenced earlier than the Eocene.

Positive fold tests show that the HTC of the Upper Cretaceous Jingzhushan Formation has a pre-folding origin. If the HTC is a secondary magnetic component, the remagnetization process very likely lasted for a short time and can be regarded as a spot reading of the geomagnetic field. Thus, the paleosecular variation test was applied to the HTC in this study. The VGP scatter (S_B) is a suitable parameter for quantifying paleosecular variation, and is defined as $S_B = \sqrt{S_T{}^2 - S_w{}^2/n}$, where $S_T = \sqrt{\sum_{i=1}^{N} \frac{\theta_i^2}{(N-1)}}$ is the angular dispersion of the VGPs about the axis of rotation (Cox, 1970), and S_w is the contribution to the dispersion that has arisen from rock magnetic and experimental errors. The n and N are the average number of samples of per sampling sites and the amount of sampling sites of sampling section, respectively. The θ_i is the angle between the ith virtual geomagnetic pole (VGP) unit vector and the spin axis. In general, a value of 14° has been used for ages exceeding 45 Ma (McFadden et al., 1991). A widely accepted method is to compare the VGP scatter with that expected by McFadden et al. (1991). Given that the HTC of the Upper Cretaceous Jingzhushan Formation should have been acquired sometime in the interval from the Later Cretaceous to the Paleocene (996–55.8 Ma), the corresponding expected VGP scatter value of 45–80 Ma (10.4–13.9 at the 95% confidence limit) and 80–110 Ma (7.0–11.3 at the 95% confidence limit) were selected for comparison. The HTC of H1 has a VGP scatter of 10.52, which falls into the expected VGP scatter interval of 45–80 Ma and 80–110 Ma, indicating that the HTC has averaged out paleosecular variation, and that it should have been acquired over a long period of time.

Furthermore, Deenen et al. (2011) provide a N-dependent A_{95} envelope (N is the number of samples used to calculated the mean direction of sampling section), bounded by an upper limit $A_{95\ \max}$ and a lower limit $A_{95\ \min}$, which can ascertain whether or not the distribution of VGP of samples has sufficiently well-sampled paleosecular variation (PSV) and therefore the samples recorded the geomagnetic field behavior of deposition process. The sample-mean VGP of sampling section is Latitude = 72.0°N, Longitude = 273.8°E, $K = 23.8$, $A_{95} = 2.4°$, which is consistent with the site-mean VGP of sampling section (Latitude = 71.4°N, Longitude = 273.1°E, $K = 23.8$, $A_{95} = 5.2)°$. The A_{95} value of the mean VGP of all 150 samples falls within the range of A_{95} values ($A_{95\ \max} = 3.5°$, $A_{95\ \min} = 2.3°$), which indicates that the Jingzhushan Formation adequately recorded the geomagnetic field of the deposition process.

Table 1
Medium-temperature magnetic components of the Upper Cretaceous Jingzhushan Formation red-beds samples collected from the Dingqing area.

Site	Locality	Bedding	n/N	In situ		Tilt-corrected		k	α_{95} (°)	Average VGP		A_{95} (°)	Rock type
	N/E(°)	Strike/dip (°)		Dec. (°)	Inc. (°)	Dec. (°)	Inc. (°)			Lat. (°N)	Lon. (°E)		
DQ2	31°13′/95°59′	282/7	10/12	38.0	33.5	36.7	27.8	18.2	11.0	–	–	–	Siltstone
DQ4	31°13′/95°59′	243/11	5/11	357.2	33.0	355.0	22.8	102.0	12.3	–	–	–	Siltstone
DQ7	31°14′/95°57′	260/21	5/14	33.7	42.7	24.5	26.3	94.4	9.5	–	–	–	Fine sandstone
DQ8	31°14′/95°57′	267/20	7/24	32.0	41.6	23.7	21.7	20.6	13.6	–	–	–	Mudstone
DQ10	31°14′/95°57′	266/26	5/11	26.6	38.9	20.3	15.7	17.1	19.1	–	–	–	Mudstone
DQ11	31°14′/95°57′	272/23	8/12	26.2	48.6	19.5	26.3	18.0	13.4	–	–	–	Mudstone
DQ12	31°14′/95°57′	269/18	6/14	10.1	41.5	8.1	23.7	94.3	6.9	–	–	–	Siltstone
DQ13	31°14′/95°57′	264/25	5/12	7.5	31.2	5.6	6.8	77.2	14.1	–	–	–	Siltstone
DQ14	31°18′/95°47′	244/73	7/10	358.9	50.4	351.7	−20.5	58.1	8.0	–	–	–	Siltstone
DQ15	31°18′/95°47′	244/73	5/10	349.3	50.0	344.5	−21.6	41.9	12.0	–	–	–	Siltstone
DQ16	31°18′/95°47′	249/77	7/12	16.2	50.2	3.1	−19.0	17.0	15.1	–	–	–	Siltstone
Mean direction			11	16.4	43.1			33.0	8.1				
			11			10.1	10.7	10.3	14.9				

Fold test: (A) negative fold test at 95% confidence limits; (B) negative fold test at 95% confidence limits
(A) McElhiny's Test: $N = 11$, $k_s/k_g = 0.31 < F[20,20] = 2.12$ at 95% confidence limit
(B) McFadden's Test: $N = 11$, $\xi_{(2)\ \text{in-situ}} = 1.35 < \xi_C = 3.86 < \xi_{(2)\ \text{tilt-corrected}} = 7.80$ at 95% confidence limit

N and n are number of samples collected and used for paleomagnetic calculation, respectively. Dec. and Inc. are declination and inclination, respectively; k is the Fisherian precision parameter for samples (Fisher, 1953); α_{95} and A_{95} are the radius of cone at 95% confidence level about the mean direction. Lat. and Lon. are latitude and longitude of paleopoles.

5.2. Inclination shallowing correction for the Upper Cretaceous Jingzhushan red-beds

Comparison of paleomagnetic data from the Mesozoic and Cenozoic red-beds with that from coeval volcanic rocks confirms that depositional and/or compaction-induced inclination shallowing in red-beds might result in inclination deviation in East Asia (Gilder et al., 2003; Tan et al., 2003; Tauxe and Kent, 2004).

The elongation/inclination (E/I) correction method of Tauxe and Kent (2004) is often used to test for inclination shallowing of red-beds. The principle of the E/I correction method is that although deposition/compaction should systematically decrease the inclination, the declination should remain stable, which would lead to flattening of the paleomagnetic data along the direction of the latitudinal line (Tauxe, 2005). However, local rotational deformation about vertical-axis, or the plunging folds, can also induce dispersion of the paleomagnetic data, and lead to false appearance that the paleomagnetic data is flatted by the deposition/compaction process (Tong et al., 2015). Thus, if the bedding of sampling strata changed complexly because of tectonic deformation, the E/I correction method would give the excessive inclination shallowing correction result.

Table 2
High-temperature magnetic components of the Upper Cretaceous Jingzhushan Formation red-beds samples collected from the Dingqing area.

Site	Locality	Bedding	n/N	In situ		Tilt-corrected		k	α_{95} (°)	Average VGP		A_{95} (°)	Rock type
	N/E(°)	Strike/dip (°)		Dec. (°)	Inc. (°)	Dec. (°)	Inc. (°)			Lat. (°N)	Lon. (°E)		
DQ1	31°13′/95°59′	304/4	8/12	357.1	25.2	358.2	22.0	70.1	6.7	70.1	281.0	5.1	Mudstone
DQ2	31°13′/95°59′	282/7	10/12	3.1	40.1	4.0	33.8	18.7	11.5	76.8	259.1	9.9	Siltstone
DQ3	31°13′/95°59′	288/9	10/12	358.2	26.6	357.8	17.2	30.2	8.9	67.5	281.5	6.6	Siltstone
DQ4	31°13′/95°59′	243/11	10/11	355.7	33.9	354.6	25.9	26.6	9.5	71.7	292.8	7.5	Siltstone
DQ5	31°13′/95°59′	227/3	8/15	351.7	26.8	351.3	23.4	24.2	11.5	69.3	300.6	8.9	Siltstone
DQ6	31°14′/95°57′	260/21	10/12	338.3	47.6	341.2	26.9	22.1	9.9	65.8	325.4	7.9	Siltstone
DQ7	31°14′/95°57′	260/21	12/14	8.8	55.0	3.0	34.8	36.0	7.0	77.6	262.5	6.1	Fine sandstone
DQ8	31°14′/95°57′	267/20	9/12	12.4	41.7	9.8	19.3	22.1	9.0	66.8	250.6	6.8	Mudstone
DQ9	31°14′/95°57′	261/24	10/12	10.4	46.4	5.5	23.4	14.4	13.2	70.3	259.7	10.3	Mudstone
DQ10	31°14′/95°57′	266/26	10/11	21.5	42.6	15.5	18.6	17.3	12.0	64.0	238.9	9.0	Mudstone
DQ11	31°14′/95°57′	272/23	10/12	22.2	47.3	16.9	24.7	22.0	10.5	66.0	231.7	8.2	Mudstone
DQ12	31°14′/95°57′	269/18	13/14	9.9	50.6	7.2	32.9	30.0	7.4	75.2	248.1	6.3	Siltstone
DQ13	31°14′/95°57′	264/25	9/12	343.8	32.5	345.3	7.8	69.0	5.5	59.4	305.6	3.9	Siltstone
*DQ14	31°18′/95°47′	244/73	10/10	90.7	13.8	59.6	25.5	21.4	10.7	32.8	189.7	8.5	Siltstone
*DQ15	31°18′/95°47′	244/73	10/10	84.6	4.8	65.4	21.0	56.2	6.5	26.6	189.1	5.0	Siltstone
*DQ16	31°18′/95°47′	249/77	10/12	90.5	1.1	72.9	21.1	11.8	14.7	20.2	185.1	11.2	Siltstone
DQ17	31°18′/95°47′	215/80	9/12	56.0	41.4	354.2	22.3	21.9	11.3	69.6	292.3	8.7	Siltstone
DQ18	31°18′/95°47′	216/75	12/13	57.8	29.1	10.6	26.1	10.1	14.4	70.0	244.4	11.5	Siltstone
H1: mean direction of DQ1–DQ13 and DQ17,18 of late Cretaceous			15	9.0	41.3			16.6	9.7				
			15			0.9	24.3	46.8	5.6	71.4	273.1	5.2	
Fold test: (A) positive fold test at 95% confidence limits; (B) positive fold test at 95% confidence limits													
(A) McElhiny's Test: $N = 15$, $k_s/k_g = 2.82 > F[28,28] = 1.88$ at 95% confidence limit													
(B) McFadden's Test: $N = 15$, $\xi_{(2)\ \text{in-situ}} = 8.25 > \xi_C = 4.51 > \xi_{(2)\ \text{tilt-corrected}} = 1.06$ at 95% confidence limit													
H2: mean direction of DQ14–DQ16 of late Cretaceous			3	88.6	6.6			120.6	11.3				
			3			66.0	22.6	148.3	10.2				
Fold test: inconclusive fold test at 95% confidence limits													
McFadden's Test: $N = 3$, $\xi_{(2)\ \text{in-situ}} = 2.68$, $\xi_C = 2.07$, $\xi_{(2)\ \text{tilt-corrected}} = 0.54$ at 95% confidence limit													
Mean inclination of H1 and H2 types			18		33.8 ± 9.5			14.0					
			18				23.7 ± 3.8	80.6					

N and n are number of samples collected and used for paleomagnetic calculation, respectively. Dec. and Inc. are declination and inclination, respectively; k is the Fisherian precision parameter for samples (Fisher, 1953); α_{95} and A_{95} are the radius of cone at 95% confidence level about the mean direction. Lat. and Lon. are latitude and longitude of paleopoles.
* means the sampling sites experienced local rotational deformation relative to the other sampling sites.

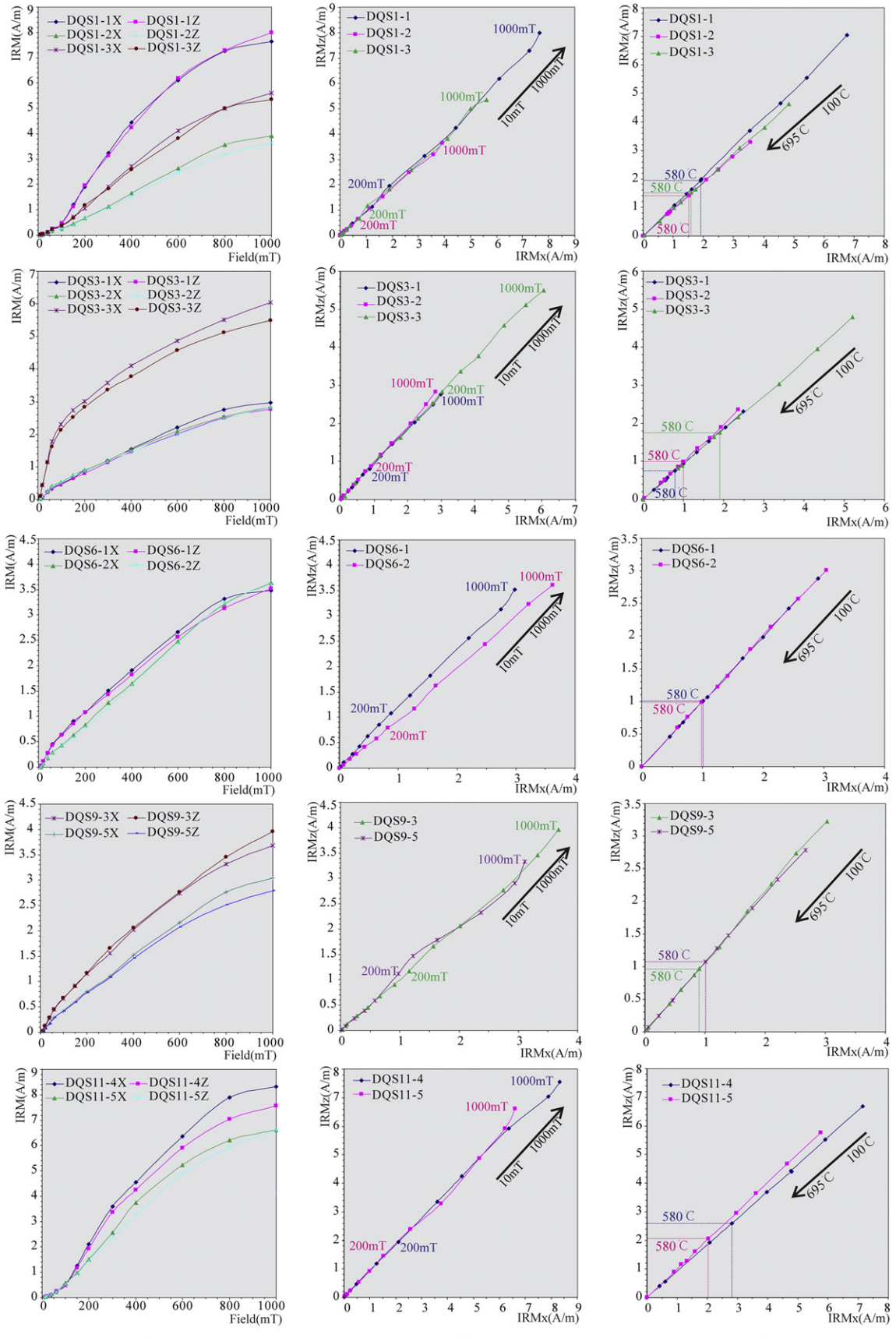
IRM(A/m)
Field(mT)
DQS1-1X
DQS1-1Z
DQS1-2X
DQS1-2Z
DQS1-3X
DQS1-3Z
IRMz(A/m)
IRMx(A/m)
DQS1-1
DQS1-2
DQS1-3
1000mT
200mT
10mT
100℃
695℃
580℃
DQS3-1X
DQS3-1Z
DQS3-2X
DQS3-2Z
DQS3-3X
DQS3-3Z
DQS3-1
DQS3-2
DQS3-3
DQS6-1X
DQS6-1Z
DQS6-2X
DQS6-2Z
DQS6-1
DQS6-2
DQS9-3X
DQS9-3Z
DQS9-5X
DQS9-5Z
DQS9-3
DQS9-5
DQS11-4X
DQS11-4Z
DQS11-5X
DQS11-5Z
DQS11-4
DQS11-5
(A)
(B)
(C)

In this work, all the sampling sites were distributed in the north limb of fold, and the beddings of DQ1–DQ13 sites are approximately consistent with each other (Fig. 1B), thus it is difficult to determine that the sampling strata experienced plunging folding. However, the declinations of DQ14–DQ16 sites were obviously different with that of other sampling sites, indicating the sampling strata should experience obviously local rotational deformation about the vertical-axis. Thus, the E/I correction method is not suitable for the paleomagnetic data of this study. The anisotropy-based inclination shallowing correction method of Hodych and Buchan (1994) can avoid the influence of tectonic deformation of sampling strata, and thus this method was used to quantitatively test the extent of inclination deviation in this study. A total 12 standard specimens were drilled from five hand samples in the direction perpendicular to the strata bedding. The values of IRM parallel (IRMx) and perpendicular (IRMz) to the bedding plane for 12 specimens were measured in successively increasing DC fields (in the range of 0–1000 mT) in the 45° ± 0.5° direction of the specimens (Fig. 6A), and subsequently thermal demagnetization (with temperatures in the range of 100–695 °C) was performed on the specimens. The values of IRMz/IRMx in the range of 200–1000 mT and in the thermal demagnetization temperature range of 100–680 °C all approximately trend to 1 (Table 3, Fig. 6B, C). The mean ratios of IRMz/IRMx with the SD (standard deviation) in the temperature interval of 580–695 °C are 0.9655 ± 0.0305 for DQ1, 0.9493 ± 0.0223 for DQ3, 0.9972 ± 0.0024 for DQ6, 1.0622 ± 0.0034 for DQ9 and 0.9552 ± 0.0331 for DQ11 (Table 3). Considering that the HTC was isolated within the temperature range 580–695 °C, the mean IRMz/IRMx in this temperature range was used to correct the inclination of the Late Cretaceous paleomagnetic data. The corrected mean inclinations for the five sampling sites are consistent with the observed inclinations (Table 3), indicating that depositional and/or compaction-induced inclination shallowing is insignificant in the Upper Cretaceous Jingzhushan Formation red-bed in the Dingqing area.

Furthermore, Cogné et al. (2013) suggest that the Eurasia was not behaved as a single rigid plate in the Mesozoic. It could induce the inclination shallowing of paleomagnetic data of the East Asia when using the APWP of Europe constructed by the paleomagnetic data of unstable Eurasia as the reference poles. Thus they constructed a new 130–0 Ma reference APWP of East Asia based on the consistency of paleomagnetic data of the Siberian Craton, Amuria, Korea, North and South China Blocks. In this work, the reference pole of East Asia (Cogné et al., 2013) was selected as reference pole for discussion, to avoid the inclination shallowing of paleomagnetic data in Tibet induced by the Cretaceous and Paleogene tectonic deformation in Europe.

6. Discussion

6.1. Filtering of the Cretaceous and Paleogene paleomagnetic data for the Lhasa Terrane

During the last three decades, considerable Cretaceous and Paleogene paleomagnetic data has been obtained from the western and central part of the Lhasa Terrane (e.g., Achache et al., 1984; Chen et al., 2010; Dupont-Nivet et al., 2010; Tan et al., 2010; Meng et al., 2012; Sun et al., 2010, 2012; Huang et al., 2013; Ma et al., 2014; Yang et al., 2014, 2015). Vand der Voo (1990) proposed the seven-criterion system to evaluate the quality of paleomagnetic data, which assigns a quality factor Q-value for paleomagnetic data. Five of the seven criteria were usually used to evaluate the quality of paleomagnetic data in previous work (Li et al., 2017): the magnetic component should be isolated from at least 50 paleomagnetic specimens by stepwise demagnetization, and meanwhile the fold tests should be positive for magnetic component and its acquisition age is well-determined. A total of 21 Cretaceous and Paleogene paleomagnetic data was selected from published studies (Table 4).

Because of the possibility of deposition and/or compaction-induced inclination shallowing of the red-beds, paleomagnetic data from the Cretaceous and Paleogene red-beds not subject to an inclination shallowing test was excluded for the subsequent discussion. In addition, the E/I correction could result in overcorrection of inclinations if the sampling area experienced intense tectonic deformation and/or regional rotational deformation about the vertical-axis. Therefore, paleomagnetic data from red-beds that had only been subjected to E/I correction was also excluded. Ma et al. (2014) and Swanson-Hysell et al. (2011) suggested that the same remanence direction carried by both magnetite and hematite in volcanic rocks indicates that both the magnetite and hematite were formed by exsolution during initial cooling, rather than by long-term low-temperature oxidation of the original Fe oxides after cooling. Although, Huang et al. (2015) suggested that the Eocene Linzizong volcanic rocks in the Nanmulin Basin experienced remagnetization and that the acquired HTC was carried by secondary growth hematite, the thin magmatic flows can easily be altered by the overlying contemporary flow and still carry a primary remanence in hematite. If the magnetic component obtained from volcanic rocks was only carried by hematite and show a single polarity, it is very important to carry out more detailed rocks magnetic test to determine the origin of the hematite and the acquisition time of the magnetic components. Thus, the HTC of volcanic rocks that only being carried by hematite and was not analyzed the origin of hematite, was excluded from the subsequent discussion. According to these additional filtering criteria, several published paleomagnetic data in Table 1 were also excluded. The Eocene and Lower Cretaceous paleomagnetic data of Tan et al. (2010) were obtained from tuffs and lava flows in the Lhasa Terrane, respectively; however, although positive fold tests indicate their pre-folding origin, the lack of rock magnetic analysis and the single polarity of the data made it difficult to determine the magnetic carrier. In addition, Tan et al. (2010) obtained Upper Cretaceous paleomagnetic data from red-beds in the central part of the Lhasa Terrane. Their sampling section was distributed in the two limbs of plunging fold, but only E/I correction was applied to the paleomagnetic data. The Lower Cretaceous paleomagnetic data of Achache et al. (1984) was obtained from two sampled sections of red-beds in the central part of the Lhasa Terrane, but their paleomagnetic data were not subjected to any inclination shallowing tests. Sun et al. (2012) obtained paleomagnetic data from Upper Cretaceous red-beds and andesite, but the HTC of andesite was only carried by hematite, and the site-mean direction of andesite was slightly different to that of the red-beds; moreover, the HTC of the red-beds was not subjected to any inclination shallowing tests. Thus, these paleomagnetic data were also excluded from the discussion. Finally, 15 paleomagnetic studies (8 for the Paleogene, 3 for the Late Cretaceous and 4 for the Early Cretaceous) were selected for the subsequent tectonic discussion (Table 4). It is noteworthy that the Eocene paleomagnetic data of Huang et al. (2013) was obtained from red-beds and tuffs in the central part of Lhasa Terrane. The HTC of the tuffs was carried by magnetite and was confirmed to be a primary magnetic component. E/I correction and anisotropy-based inclination correction indicate that compaction-induced inclination shallowing occurs in the red-beds. Thus, their paleomagnetic data after inclination shallowing correction was used in the discussion (Table 4).

6.2. Paleolatitude of the Lhasa Terrane in the Cretaceous and Paleogene

The Lhasa Terrane is a narrow E-W extended block with a length of more than 2000 km, which composed the southern edge of the Eurasia

Fig. 6. (A): Plots of IRMx (parallel to bedding) and IRMz (perpendicular to bedding) acquisitions produced by applying a magnetic field at an angle of 45° to the bedding as a function of increasing field. (B): The slope (IRMz/IRMx) of the least-squares-fit for the data points between 200 mT and 1000 mT was used to estimate the magnetic anisotropy of hematite. (C): The slope of the thermal demagnetization of IRMz and IRMx between 580 °C and 680 °C was used to estimate the inclination shallowing ratio for the inclination correction of the red-bed samples.

Table 3
Anisotropy of isothermal remanent magnetization of the Upper Cretaceous Jingzhushan Formation red-beds samples collected from the Dingqing area.

Site	Name	I_{obs} (sampling sites)	I_F	IRMz/IRMx (acquired between 200 and 1000 mT)	IRMz/IRMx		Average IRMz/IRMx (acquired above 580 °C) and its standard deviation
					100–695 °C	Acquired above 580 °C	
DQ1	DQS1–1	22.0	22.7	1.0428	1.0325	1.0113	0.9655 ± 0.0305
	DQS1–2			0.9016	0.9257	0.9336	
	DQS1–3			0.9477	0.9538	0.9517	
DQ3	DQS3–1	17.2	18.1	0.9098	0.9260	0.9371	0.9493 ± 0.0223
	DQS3–2			0.9964	0.9893	0.9827	
	DQS3–3			0.8939	0.9137	0.928	
DQ6	DQS6–1	26.9	26.9	0.9856	0.9921	0.9995	0.9972 ± 0.0024
	DQS6–2			1.0195	0.9948	0.9948	
DQ9	DQS9–3	23.4	22.2	1.0773	1.0769	1.0655	1.0622 ± 0.0034
	DQS9–2			0.9407	1.0511	1.0588	
DQ11	DQS11–4	24.7	25.7	0.8895	0.9312	0.9221	0.9552 ± 0.0331
	DQS11–5			0.9966	1.0028	0.9883	

Name: the ID of the specimens used for the inclination shallowing testing; I_{obs}: Observed mean inclination of sampling sites; I_F: means inclination calculated from the IRMz/IRMx acquired above 580 °C.

prior to the collision of Indian plate and the Eurasia. Although many paleomagnetic data were obtained from the Cretaceous and Paleogene red-beds and volcanic rocks in the Lhasa Terrane, only two Upper Cretaceous paleomagnetic studies (Tang et al., 2013; Yang et al., 2014) can be used to restrict the paleolatitude of the Lhasa Terrane, because of lacking inclination shallowing test of red-beds and potential re-magnetization of volcanic for most of paleomagnetic studies (Table 4). Furthermore, the two paleomagnetic data were obtained from the western part of the Lhasa Terrane (GPS position of sampling section are 31.2°N/84.7°E and 30.6°N/85.2°E), but the Upper Cretaceous paleomagnetic data from the Tethyan Himalaya were obtained from the central part of it (GPS position of sampling section is 28.3°N/88.5°E). It is inappropriate to assign the paleolatitude of the southern edge of Eurasia prior to the collision of Indian plate and Eurasia according to paleomagnetic data from the western part of the Lhasa Terrane. The paleomagnetic data of this study supplements the scarcity database of the Upper Cretaceous paleomagnetic data of Lhasa Terrane. Then, combining the Upper Cretaceous paleomagnetic data of the western and eastern part of the Lhasa can more reasonably restrict the paleolatitude of the southern edge of the Eurasia prior to the collision of Indian plate and Eurasia. A reference point (29.0°N, 87.5°E) located in the middle segment of the Indus-Tsangpo suture zone was used to calculate the paleolatitudes of the sampling area (Yang et al., 2015).

The small-circle fitting method of Mardia and Gadsden (1977) was used to fit the filtered Early Cretaceous, Late Cretaceous and Paleocene poles. The fitting small-circle result passes through 8 selected Paleogene poles (Achache et al., 1984; Chen et al., 2010; Dupont-Nivet et al., 2010; Liebke et al., 2010; Sun et al., 2010; Meng et al., 2012; Huang et al., 2013) and gives a colatitude of 74.8° ± 5.0°N centered on the reference point (29.0°N, 87.5°E). This indicates that the reference point was situated at the paleolatitude of 15.2° ± 5.0°N, in the Paleogene (Fig. 7A). The same method was applied to the Late Cretaceous and Early Cretaceous poles. The fitting small-circle results pass through 3 Late Cretaceous poles (Tang et al., 2013; Yang et al., 2014; This study) and 4 Early Cretaceous poles (Chen et al., 2012; Ma et al., 2014; Yang et al., 2014; Li et al., 2017), with colatitudes of 79.2° ± 6.7°N and 76.8° ± 8.6°N, respectively. This indicates that reference point (29.0°N, 87.5°E) was situated at the paleolatitude of 10.8° ± 6.7°N in the Late Cretaceous (Fig. 7B), and at the paleolatitude of 13.2° ± 8.6°N in the Early Cretaceous (Fig. 7C).

6.3. Timing of the India-Eurasia collision

Previous geological studies have indicated that the Lhasa Terrane remained stationary from the Early Cretaceous to the Paleocene, and that it comprised the stable southern edge of Eurasia prior to the collision of India-Eurasia (Kapp et al., 2003, 2007; Chen et al., 2010; Sun et al., 2010, 2012; Zhu et al., 2011; Chen et al., 2012; Tang et al., 2013; Lippert et al., 2014; Ma et al., 2014, Yang et al., 2014). The Tethyan Himalaya represented the northernmost margin of Greater India, before the collision of India and Eurasia (Patzelt et al., 1996; Yi et al., 2011; Sun et al., 2010; Ma et al., 2014; Li et al., 2017). Thus, comparison of the paleolatitudes of the Lhasa Terrane and the Tethyan Himalaya can potentially provide constraints on the timing of the collision of India-Eurasia.

Published Cretaceous and Paleogene paleomagnetic data for Tethyan Himalaya were selected to estimate its paleolatitude (Table 4). The Early Cretaceous and Late Cretaceous paleomagnetic data for the Tethyan Himalaya were obtained from the Lakang Formation lava flow (134–131 Ma) (Yang et al., 2015) and the Zongshan Formation limestone (71–65 Ma) (Patzelt et al., 1996). The data show that the Tethyan Himalaya was situated at the paleolatitude of 48.1° ± 5.7°S from 134 to 131 Ma and at 5.1° ± 3.5°S from 71 to 65 Ma (reference point: 29.0°N, 87.5°E) (Fig. 7B, C). Four Paleogene paleomagnetic data for Tethyan Himalaya were obtained from the Paleogene Zongpu Formation limestone (63–55 Ma) (Patzelt et al., 1996; Yi et al., 2011; Yang et al., 2014). Because the ages of the paleomagnetic data of Yang et al. (2014) and Patzelt et al. (1996) span a wide range (63–55 Ma), their Paleogene paleomagnetic data were not used to constrain the paleolatitude of the Tethyan Himalaya. The Paleogene paleomagnetic data of Yi et al. (2011) show that the Tethyan Himalaya was situated at the paleolatitude of 6.3° ± 3.5°N from 62 to 59 Ma, and that subsequently it drifted to 10.9° ± 2.5°N from 59 to 56 Ma (Fig. 7B).

The Tethyan Himalaya moved progressively from a high southern latitude (48.1° ± 5.7°S) from 134 to 131 Ma to a low northern latitude of 10.9° ± 2.5°N from 59 to 56 Ma. The gap between the Tethyan Himalaya at the northernmost edge of Great India and the Lhasa Terrane was about 61.3° ± 10.3° (~6700 ± 1100 km) in the Early Cretaceous and 15.9° ± 7.5° (~1700 ± 825 km) in the Late Cretaceous (Fig. 7B, C). The Paleogene paleomagnetic data of the Lhasa Terrane were obtained from red-beds and volcanic rocks with the wide time range of 64–43 Ma, part of which very likely post-dates the collision of India-Eurasia. Thus, the Paleogene latitude of the Lhasa Terrane is unsuitable for constraining the collision time of India and Eurasia (Li et al., 2017). In addition, the Tethyan Himalaya was closer to the Lhasa Terrane in the Late Cretaceous than in the Early Cretaceous. Thus, the Late Cretaceous paleomagnetic data for the Lhasa Terrane and the Tethyan Himalaya are more suitable for constraining the collision time of India and Eurasia. The southern edge of the Lhasa Terrane was situated at a paleolatitude of 10.8° ± 6.7°N in the Late Cretaceous, which represented the southern margin of Eurasia prior to the collision of India-Eurasia (Fig. 8). The Tethyan Himalaya was situated at the paleolatitude of 5.1° ± 3.5°S from 71 to 65 Ma (Patzelt et al., 1996); it then, drifted to 6.3° ± 3.5°N from 62 to 59 Ma (60.5 ± 1.5 Ma) (Yi et al., 2011), and finally 10.9° ± 2.5°N in 59–56 Ma (57.5 ± 1.5 Ma) (Yi et al., 2011) (Fig. 8). The paleolatitude of the Tethyan Himalaya (6.3° ± 3.5°N) began to overlap with that of the Lhasa Block (10.8° ± 6.7°N) at the 60.5 ± 1.5 Ma, and since the 57.5

Table 4
The Cretaceous and Paleocene paleomagnetic poles from the Lhasa Terrane and the Tethyan Himalaya.

Site (°N/°E)	Time (Ma)	N	Observed			Paleopole			Paleolat. (°)	Rock type	Fold test	Inclination shallowing correction	Magnetic carrier	Reference
			Dec. (°)	Inc. (°)	α_{95} (°)	Plat. (°)	Plon. (°)	A_{95} (dp/dm)						
Lhasa Terrane														
#30.0/91.2	E (43-40)	9	359.5	51.8	5.2	87.5	81.4	5.9	31.5 ± 5.9	T	P	—	No magnetic rock analysis	Tan et al., 2010
30.0/91.2	E (54-43)	—	10.2	40.0	2.6	78.4	217.2	2.6	21.3 ± 2.6	R + T	M	E/I + A	Magnetite for tuff	Huang et al., 2013
30.0/91.1	E (53)	9	13.4	30.8	6.3	71.8	225.7	5.7	14.9 ± 5.7	D	P + D	—	Titanomagnetite	Liebke et al., 2010
30.0/91.1	E (54-47)	24	12.5	39.4	5.3	76.4	212.6	5.0	20.7 ± 5.0	V	P	—	Magnetite	Dupont-Nivet et al., 2010
30.0/91.0	E	8	350.9	25.5	11.0	71.4	299.8	11.0	12.9 ± 11.0	V	P + D	—	Magnetite	Achache et al., 1984
29.9/84.3	P-E (57-54)	62	348.1	42.0	7.1	78.0	329.0	5.9	22.8 ± 5.9	S + Li + T	P	S	Magnetite for tuff	Meng et al., 2012
29.9/90.2	P-E (60-44)	23	355.9	20.2	6.9	70.6	281.0	5.3	10.1 ± 5.3	R + T + A + Li	P	—	Magnetite for tuff and andesite	Chen et al., 2010
30.1/90.9	P (56.5)	14	359.0	26.1	9.2	73.6	274.3	7.3	12.7 ± 7.3	T	P	—	MAGNETITE	Sun et al., 2010
29.7/89.2	P (64–60)	15	353.5	14.8	8.8	66.0	284.9	8.5	5.9 ± 8.5	A + T	P	—	MAGNETITE	Chen et al., 2010
31.3/95.9	K2	15	0.9	24.3	5.6	71.4	273.1	5.2	10.5 ± 5.2	R	P	A	—	This study
31.2/84.7	K2	33	316.8	30.2	5.4	49.0	344.3	5.3	13.6 ± 5.3	R	P	S	—	Yang et al., 2014
30.6/85.2	K2(99-93)	14	16.2	17.7	5.6	63.1	224.6	5.1	8.2 ± 5.1	A	P	—	Magnetite	Tang et al., 2013
#29.9/90.7	K2	20	350.8	32.1	8.1	75.0	306.7	6.8	17.0 ± 6.8	R + A	P	—	Hematite for andesite	Sun et al., 2012
#29.9/91.2	K2	43	350.2	23.5	2.5	70.2	300.5	2.2	12.0 ± 2.2	R	P	E/I	—	Tan et al., 2010
#29.9/91.2	K2	21	202.6	−41.9	4.4	69.1	191.7	4.2	22.1 ± 5.9	La	P	—	No magnetic rock analysis and only hematite can be determined	Tan et al., 2010
31.1/84.4	K1 (121.0-117.0)	12	350.5	25.5	7.7	70.5	292.9	7.4	11.1 ± 7.4	V	D	—	Magnetite	Yang et al., 2014
32.3/82.6	K1 (132-120)	51	28.2	34.5	2.3	61.4	192.9	2.1	18.3 ± 2.1	La	P	—	Hematite and magnetite	Ma et al., 2014
31.3/85.1	K1 (130.0-110.0)	18	327.0	35.7	4.6	58.2	341.8	4.6	16.7 ± 4.6	L + T	P	—	Magnetite for tuff hematite and magnetite for lava	Chen et al., 2012
30.0/91.1	K1 (120.2 ± 0.5)	19	356.4	16.4	6.3	66.9	281.2	6.1	6.5 ± 6.1	R + V	P	S	Hematite and magnetite for volcanic	Li et al., 2017
#29.9/91.1	K1	8	354.3	22.6	8.3	71.2	288.4	7.9	11.3 ± 7.9	Rb	P	No	—	Achache et al., 1984
#31.7/91.5	K1	7	337.8	27.0	8.1	63.4	326.2	5.9	13.3 ± 5.9	Rb	P	No	—	Achache et al., 1984
Tethyan Himalaya														
28.3/88.5	P (59–56)	14	357.0	19.6	3.5	71.6	277.8	2.5	10.9 ± 2.5	L	PFT	—	—	Yi et al., 2011
#28.3/88.5	P (63–55)	14	356.8	13.2	4.3	68.2	277.1	3.1	7.5 ± 3.1	L	PFT	—	—	Patzelt et al., 1996
28.3/88.5	P (62–59)	18	0.9	11.1	4.2	67.3	266.3	3.5	6.3 ± 3.5	L	PFT	—	—	Yi et al., 2011
#28.3/89.2	P (63–55)	46	359.5	12.7	3.1	68.1	270.5	2.4	7.1 ± 2.4	L	PFT	—	—	Yang et al., 2014
28.3/88.5	K2 (71–65)	14	3.9	−11.8	4.9	55.8	261.6	3.5	-5.1 ± 3.5	L	PFT	—	—	Patzelt et al., 1996
28.1/92.4	K1 (134–131)	31	261.6	−68.5	3.6	−26.8	315.2	5.7	−48.1 ± 5.7	La	PFT	—	—	Yang et al., 2015
APWP of Eurasia	60					81.9	247.5	4.1						Cogné et al., 2013

N is the number of sampling sites used for paleomagnetic calculation. Dec. and Inc. are declination and inclination, respectively. Plat. and Plon. are latitude and longitude of paleopoles. α_{95} and A_{95} is the radius of cone at 95% confidence level about the mean direction. Paleolat. is the paleolatitude calculated for the reference point at 29.0°N, 87.5°E, positive means the north latitude, negative means the south latitude. # means the paleomagnetic data were not used in the discussion. Time (Ma): K2, Late Cretaceous. K1, Early Cretaceous. P, Paleocene. E, Eocene. Rock type: R. Red-beds; S, sandstone; Li, limestone; La, lava flow; V, volcanic rock; T, tuff; D, dyke; A, Andesite. Fold Test: P, positive fold test; M, the A_{95} value of the mean VGP of sampling section falls just within the range of A_{95} values defined as a reliability envelope by Deenen et al. (2011); D, coexistence of dual-polarity. Inclination shallowing correction: E/I, E/I inclination shallowing correction; A, anisotropy-based inclination correction; S, consistent with the paleomagnetic data obtained from volcanic rocks in the same study.

± 1.5 Ma, the paleolatitude of them (10.9° ± 2.5°N for the Tethyan Himalaya and 10.8° ± 6.7°N of the Lhasa Terrane) finally overlapped together, indicating that the initial collision of India and Eurasia occurred at the paleolatitude of 10.8° ± 6.7°N, at 60.5 ± 1.5 Ma (Fig. 8).

Numerous geological observations in the Tibetan Plateau also indicated that the collision of Indian plate and Eurasia occurred in the Paleocene. The cessation of marine sedimentation at 55–50 Ma in the Tethyan Himalaya may provide a minimum age for the initial collision of the

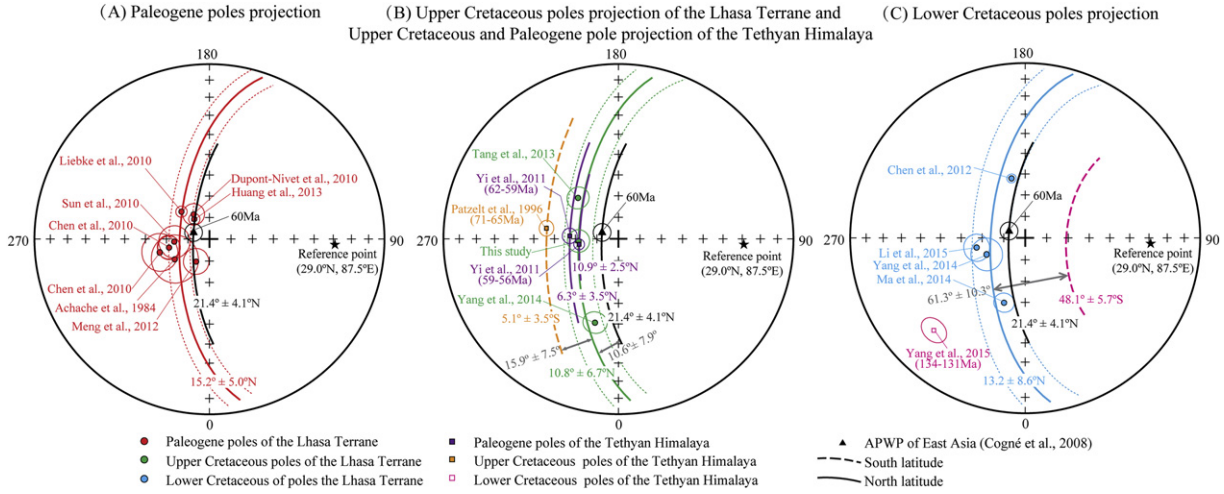

Fig. 7. (A) Equal-area projection of the Paleogene paleopoles from the Lhasa Terrane and the Tethyan Himalaya, and the reference pole of East Asia with the age of 60 Ma. Small-circle fitting passes through 8 selected Paleogene poles of the Lhasa Terrane, indicating a paleolatitude of 15.2° ± 5.0°N for the Lhasa Terrane. The expected Paleogene poles of the reference point (29.0°N, 87.5°E) is 21.4° ± 4.1°N. (B) Equal-area projection of the Late Cretaceous paleopoles from the Lhasa Terrane, and the Late Cretaceous and Paleogene paleopoles from the Tethyan Himalaya. Small-circle fitting passes through 3 selected Late Cretaceous poles of the Lhasa Terrane, and gives a paleolatitude of 10.8° ± 6.7°N for the Lhasa Terrane. The Late Cretaceous and the Paleogene paleolatitudes of the Tethyan Himalaya were also calculated using the reference point of 29.0°N, 87.5°E. (C) Equal-area projection of the Early Cretaceous paleopoles from the Lhasa Terrane and the Tethyan Himalaya. Small-circle fitting passes through 4 selected Early Cretaceous poles of the Lhasa Terrane, and gives a paleolatitude of 13.2° ± 8.6° for the Lhasa Terrane. The Early Cretaceous paleolatitude of the Tethyan Himalaya was also calculated using the reference point of 29.0°N, 87.5°E.

Indian plate and the Lhasa Terrane (Rowley, 1998; Green et al., 2008; Najman et al., 2010). The northward drift velocity of the Indian plate was reduced rapidly during the interval of 55–50 Ma, which is thought to have been caused by the collision of India and Asia (Klootwijk et al., 1992; Molnar and Stock, 2009; Copley et al., 2010; Cande and Stegman, 2011; van Hinsbergen et al., 2011). The composition of clastic sediment along the northern edge of the Indian plate changed significantly from India-derived to Asia-derived during the Late Paleocene to Early Eocene, indicating that the Indian plate was connected with Eurasia (Hu et al., 2015; DeCelles et al., 2014; Orme et al., 2014). In addition, continental synorogenic sedimentation along the ITSZ was initiated at ~55 Ma (Searle et al., 1987; Ding, 2003). The collision time indicated by geological evidence is slightly later than that of paleomagnetic data, which should be induced by the delayed effects of depositional environmental variation and tectonic response of the southern edge of Eurasia, to the initial collision of Indian plate and Eurasia.

6.4. Intracontinental crustal shortening at the southern edge of Eurasia

Abundant geological evidence indicates that the Lhasa Terrane split from the Gondwana super-continent in the interval from the Middle

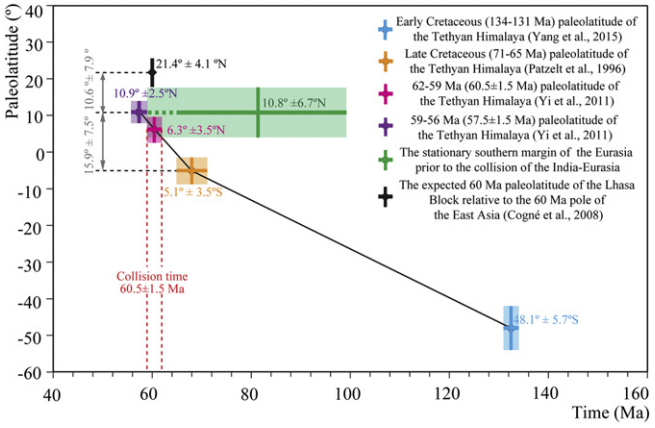

Fig. 8. Paleolatitude evolution of the Lhasa Terrane and the Tethyan Himalaya in the period of the Early Cretaceous and the Paleogene. The paleolatitudes were calculated using the reference point 9.0°N, 87.5°E.

to the Late Triassic (Metcalfe, 2009; Zhu et al., 2011), and accreted onto the Qiangtang Terrane along the Bangong-Nujiang Suture in the interval from the Late Jurassic to the Early Cretaceous (Dewey et al., 1989; Kapp et al., 2003, 2007; Guynn et al., 2006; Qiangba et al., 2009; Zhu et al., 2013). Subsequently, the Indian plate collided with Eurasia at 57.5 ± 1.5 Ma, which induced enormous crustal shortening in south Eurasia (Tapponnier et al., 1982; Royden et al., 1997; Meyer et al., 1998; Yin and Harrison, 2000; DeCelles et al., 2002; Spurlin et al., 2005; Yin et al., 2007).

Many previous paleomagnetic studies have estimated the latitudinal crustal convergence in south Eurasia since the Indian and Eurasian collision, with a ranges from ~2400 km (Sun et al., 2010; Tang et al., 2013; Ma et al., 2014; Li et al., 2017) to less than 200 km (Tan et al., 2010). Thus, the amount of post-collision crustal convergence in south Eurasia is still highly controversial. This controversy is mainly caused by the deviation of the Cretaceous and Paleogene paleomagnetic data for the Lhasa Terrane. Although recently published more reliable paleomagnetic data, based on high-quality evaluation criteria (Vand der Voo, 1990), are used to estimate the amount of latitudinal crustal convergence of south Eurasia, the estimates of post-collision latitudinal crustal convergence still range from 1740 ± 670 km (Li et al., 2017) to 780 ± 240 km (Yang et al., 2014).

We further evaluated the published paleomagnetic data according to the reliability of the inclination shallowing correction of the red-beds and the possible remagnetization of volcanic rocks indicated by the magnetic carrier of their HTC. In addition, the Late Cretaceous paleolatitude of the Lhasa Terrane was used to constrain the collision time of India and Eurasia, in order to provide a better estimate of the post-collision latitudinal crustal convergence in south Eurasia. The foregoing discussion in Section 6.2 confirmed that the initial collision of India and Eurasia occurred at the paleolatitude of 10.8° ± 6.7°N, in 60.5 ± 1.5 Ma. In this work, the reference pole of East Asia (Cogné et al., 2013) with the age of 60 Ma (81.9°N, 247.5°E, A_{95} = 4.1°), was selected to calculate the Paleogene paleolatitude of reference point (29.0°N, 87.5°E) (Table 4). The expected paleolatitude of the Lhasa Terrane calculated from the 60 Ma Eurasia reference pole is 21.4° ± 4.1°N, which shows that 10.6° ± 7.9°(1300 ± 910 km) latitudinal crustal convergence occurred across south Eurasia, since the initial collision of the Indian plate and Eurasia (Fig. 8).

Kapp et al. (2005) suggest that series of Cenozoic crustal deformation induced more than 470 km N-S crustal shortening across the

Lhasa and Qiangtang Terranes, since the Early Cretaceous. Volkmer et al. (2007) further estimate that ~46% of the 470 km N-S crustal shortening (~220 km) occurred within the Lhasa Terrane since the Paleocene. In the north side of the Lhasa Terrane, the Shiquanhe-Gaize-Amdo Thrust system and the Fenghuoshan-Nangqian fold belt in the Qiangtang Terrane, and the Qimen Tagh-North Kunlun thrust system and the Nan Shan thrust system in the Qaidam Basin have further absorbed ~900 km crustal shortening, since the collision of Indian plate and Eurasia (Meyer et al., 1998; Yin and Harrison, 2000; DeCelles et al., 2002; Spurlin et al., 2005; Yin et al., 2007; van Hinsbergen et al., 2011). The geological evidences suggest that ~1120 km crustal shortening was absorbed by the crustal deformation across the Tibetan orogeny since the Paleocene. Halls (2013) also summarized the geological and paleomagnetic evidences and estimated that the intra-continental crustal shortening across the Tibetan orogen since the ~130 Ma is at least ~1700 km. If considering that ~54% of the 470 km N-S crustal shortening (~250 km) occurred within the Lhasa Terrane in the period of Late Cretaceous and Paleocene (Volkmer et al., 2007), the estimation of Halls (2013) is consistent with that of this studies. The vast majority of post-collision latitudinal crustal convergence across south Eurasia was accommodated by the Cenozoic folding and thrust faulting system between the Lhasa Terrane and the Hexi Corridor.

7. Conclusions

(1) The primary magnetic component was isolated from the Upper Cretaceous Jingzhushan Formation red-beds in the Dingqing area, on the northeastern edge of the Lhasa Terrane, Tibetan Plateau. The tilt-corrected site-mean direction is $D_s/I_s = 0.9°/24.3°$, with $k = 46.8$, $\alpha_{95} = 5.6°$, corresponding to a pole at *Plat./Plon.* = 71.4°/273.1°, with $A_{95} = 5.2$.

(2) The Late Cretaceous paleolatitude of the southern edge of the Lhasa Terrane (10.8° ± 6.7°N) represented the southern margin of Eurasia prior to the collision of India-Eurasia. The initial collision of India-Eurasia occurred at 60.5 ± 1.5 Ma, at the paleolatitude of 10.8° ± 6.7°N.

(3) The paleolatitudinal difference between the Lhasa Terrane and the 60 Ma East Asia reference pole is 10.6° ± 7.9°, indicating that 1300 ± 910 km latitudinal crustal convergence occurred across south Eurasia, since the initial collision of India and Eurasia. The vast majority of post-collision latitudinal crustal convergence across south Eurasia was accommodated by the Cenozoic folding and thrust faulting system between the Lhasa Terrane and the Hexi Corridor.

Acknowledgements

This work was supported by the Basic Science Foundation of Chinese Academy of Geological Sciences (Grant YYWF201613) and the National Natural Science Foundation of China (Grant 41572183).

References

Achache, J., Courtillot, V., Zhou, Y.X., 1984. Paleogeographic and tectonic evolution of southern Tibet since middle Cretaceous time: new paleomagnetic data and synthesis. Journal of Geophysical Research 89, 10311–10339.

Aitchison, J., Ali, J.R., Davis, A.M., 2007. When and where did India and Asia collide? Journal of Geophysical Research 112, B05423. http://dx.doi.org/10.1029/2006JB004706.

Beck, R.A., Durbank, D.W., Sercombe, W.J., Riley, G.W., Barndt, J.K., Jurgen, H., Metjle, J., Cheema, A., Shafique, N.A., Lawrence, R.D., Khan, M.A., 1995. Stratigraphic evidence for an early collision between northwest India and Asia. Nature 373, 55–58.

BGMRX, 1993. Regional Geology of Xizang (Tibet) Autonomous Region. Geological Memoirs Series 1, 3. Geological Publishing House, Beijing.

Cai, F.L., Ding, L., Yue, Y.H., 2011. Provence analysis of upper Cretaceous strata in the Tethys Himalaya, southern Tibet: implications for timing of India-Asia collision. Earth and Planetary Science Letters 305:195–206. http://dx.doi.org/10.1016/j.epsl.2011.02.055.

Cande, S.C., Stegman, D.R., 2011. Indian and African plate motions driven by the push force of the Reunion plume head. Nature 475, 47–52.

Chen, J.S., Huang, B.C., Sun, L.S., 2010. New constraints to the onset of the India–Asia collision: paleomagnetic reconnaissance on the Linzizong Group in the Lhasa Terrane, China. Tectonophysics 489, 189–209.

Chen, W.W., Yang, T.S., Zhang, S.H., Yang, Z.Y., Li, H.Y., Wu, H.C., Zhang, J.H., Ma, Y.M., Cai, F.L., 2012. Paleomagnetic results from the Early Cretaceous Zenong Group volcanic rocks, Cuoqin, Tibet, and their paleogeographic implications. Gondwana Research 22, 461–469.

Cogné, J.P., Besse, J., Chen, Y., Hankard, F., 2013. A new Late Cretaceous to Present APWP for Asia and its implications for paleomagnetic shallow inclinations in Central Asia and Cenozoic Eurasian plate deformation. Geophysical Journal International 192, 1000–1024.

Copley, A., Avouac, J.P., Royer, J.Y., 2010. The India-Asia collision and the Cenozoic slowdown of the India plate: implications for the forces. Journal of Geophysical Research 115, B03410. http://dx.doi.org/10.1029/2009JB006634.

Cox, A., 1970. Latitude dependence of the angular dispersion of the geomagnetic field. Geophysical Journal of the Royal Astronomical Society 20:253–269. http://dx.doi.org/10.1111/j.1365-246X.1970.tb06069.x.

DeCelles, P.G., Robinson, D.M., Zandt, G., 2002. Implications of shortening in the Himalayan fold-thrust belt for uplift of the Tibetan Plateau. Tectonics 21:1062. http://dx.doi.org/10.1029/2001TC001322.

DeCelles, P.G., Kapp, P., Gehrels, G.E., Ding, L., 2014. Paleocene-Eocene foreland basin evolution in the Himalaya of southern Tibet and Nepal: implications for the age of initial India-Asia collision. Tectonics 33:824–849. http://dx.doi.org/10.1002/2014TC003522.

Deenen, M.H.L., Langereis, C.G., van Hinsbergen, D.J.J., Biggin, A.J., 2011. Geomagnetic secular variation and the statistics of palaeomagnetic directions. Geophysical Journal International 186 (2):509–520. http://dx.doi.org/10.1111/j.1365-246X.2011.05050.x.

Dewey, J.F., Cande, S., Pitman, W.C., 1989. Tectonic evolution of the India/Eurasia collision zone. Eclogae Geologicae Helvetiae 82, 717–734.

Ding, L., 2003. Paleocene deep-water sediments and radiolarian faunas: implications for evolution of Yarlung-Zangbo foreland basin, southern Tibet. Science China Earth Sciences 46, 84–96.

Dupont-Nivet, G., Lippert, P.C., Van Hinsbergen, D.J.J., Meijers, M.J.M., Kapp, P., 2010. Palaeolatitude and age of the Indo-Asia collision: palaeomagnetic constraints. Geophysical Journal International 182, 1189–1198.

Fisher, R.A., 1953. Dispersion on a sphere. Proceedings of the Royal Society of London, Series A 217, 295–305.

Gilder, S.A., Chen, Y., Cogné, J.P., Tan, X., Courtillot, V., Sun, D., Li, Y., 2003. Paleomagnetism of Upper Jurassic to Lower Cretaceous volcanic and sedimentary rocks from the western Tarim Basin and implications for inclination shallowing and absolute dating of the M-0 (ISEA?) chron. Earth and Planetary Science Letters 206, 587–600.

Gilder, S.A., Gomez, J., Chen, Y., Cogne, J.P., 2008. A new paleogeographic configuration of the Eurasian landmass resolves a paleomagnetic paradox of the Tarim Basin (China). Tectonics 27, TC1012. http://dx.doi.org/10.1029/2007TC002155.

Green, O.R., Searle, M.P., Corfield, R.I., Corfield, R.M., 2008. Cretaceous-Tertiary carbonate platform evolution and the age of the India-Asia collision along the Ladakh Himalaya (Northwest India). Journal of Geology 116 (4):331–353. http://dx.doi.org/10.1086/588831.

Guynn, J.H., Kapp, P., Pullen, A., Gehrels, G., Heizler, M., Ding, L., 2006. Tibetan basement rocks near Amdo reveal "missing" Mesozoic tectonism along the Bangong suture, central Tibet. Geology 34, 505–508.

Halls, H., 2013. Crustal shortening during the Paleoproterozoic: can it be accommodated by paleomagnetic data? Precambrian Research 244 (1), 42–52.

van Hinsbergen, D.J.J., Kapp, P., Dupont-Nivet, G., Lippert, P.C., DeCelles, P.G., Torsvik, T.H., 2011. Restoration of Cenozoic deformation in Asia and the size of Greater India. Tectonics 30, TC5003. http://dx.doi.org/10.1029/2011TC002908.

Hodych, J.P., Buchan, K.L., 1994. Early Silurian palaeolatitude of the Springdale Group redbeds of central Newfoundland: a palaeomagnetic determination with a remanence anisotropy test for inclination error. Geophysical Journal International 117, 640–652.

Hu, X.M., Wang, J.G., BouDagher-Fadel, M., Garzanti, E., An, W., 2015. New insights into the timing of the India-Asia collision from the Paleogene Quxia and Jialazi formations of the Xigaze forearc basin, south Tibet. Gondwana Research http://dx.doi.org/10.1016/j.gr.2015.02.007.

Huang, W.T., Dupont-Nivet, G., Lippert, P.C., van Hinsbergen, D.J.J., Hallot, E., 2013. Inclination shallowing in Eocene Linzizong sedimentary rocks from Southern Tibet: correction, possible causes and implications for reconstructing the India–Asia collision. Geophysical Journal International 194, 1390–1411.

Huang, W., van Hinsbergen, D.J.J., Dekkers, M.J., Garzanti, E., Dupont-Nivet, G., Lippert, P.C., Li, X., Maffione, M., Langereis, C.G., Hu, X., Guo, Z., Kapp, P., 2015. Paleolatitudes of the Tibetan Himalaya from primary and secondary magnetizations of Jurassic to Lower Cretaceous sedimentary rocks. Geochemistry, Geophysics, Geosystems 16. http://dx.doi.org/10.1002/2014GC005624.

International Association of Geomagnetism and Aeronomy, Working Group V-MOD, 2010. International Geomagnetic Reference Field: the eleventh generation. Geophysical Journal International 183, 1216–1230.

Jaeger, J.J., Courtillot, V., Tapponnier, P., 1989. Paleontological view of the ages of the Deccan traps, the Cretaceous/Tertiary boundary, and the India–Asia collision. Geology 17, 316–319.

Kapp, P., Murphy, M.A., Yin, A., Harrison, T.M., Ding, L., Guo, J.R., 2003. Mesozoic and Cenozoic tectonic evolution of the Shiquanhe area of western Tibet. Tectonics 22 (1029). http://dx.doi.org/10.1029/2001TC001332.

Kapp, P., Yin, A., Harrison, T.M., Ding, L., 2005. Cretaceous-Tertiary shortening, basin development, and volcanism in central Tibet. Geological Society of America Bulletin 117, 865–878.
Kapp, P., DeCelles, P.G., Gehrels, G.E., Heizler, M., Ding, L., 2007. Geological records of the Lhasa–Qiangtang and Indo-Asian collisions in the Nima area of central Tibet. GSA Bulletin 119, 917–932.
Kirschvink, J.L., 1980. The least-squares line and plane and the analysis of palaeomagnetic data. Geophysical Journal of the Royal Astronomical Society 62, 699–718.
Klootwijk, C.T., Gee, J.S., Peirce, J.W., Smith, J.M., McFadden, P.L., 1992. An early India-Asia contact: paleomagnetic constraints from Ninetyeast Ridge, ODP Leg 121. Geology 20, 395–398.
Li, Z.Y., Ding, L., Song, P.P., Fu, J.J., Yue, Y.H., 2017. Paleomagnetic constraints on the paleolatitude of the Lhasa Terrane during the Early Cretaceous: implications for the onset of India-Asia collision and latitudinal shortening estimates across Tibet and stable Asia. Gondwana Research 41:352–372. http://dx.doi.org/10.1016/j.gr.2015.05.013.
Liebke, U., Appel, E., Ding, L., Neumann, U., Antolin, B., Xu, Q., 2010. Position of the Lhasa terrane prior to India–Asia collision derived from palaeomagnetic inclinations of 53 Ma old dykes of the Linzhou Basin: constraints on the age of collision and post-collisional shortening within the Tibetan Plateau. Geophysical Journal International 182, 1199–1215.
Lippert, P.C., van Hinsbergen, D.J.J., Dupont-Nivet, G., 2014. The Early Cretaceous to Present latitude of the central Lhasa-plano: a paleomagnetic synthesis with implications for Cenozoic tectonics, paleogeography, and climate of Asia. In: Nie, J.S., Hoke, G.D., Horton, B.K. (Eds.), Towards an Improved Understanding of Uplift Mechanisms and the Elevation History of the Tibetan Plateau. Geological Society of America Special Paper 507.
Lowrie, W., 1990. Identification of ferromagnetic minerals in a rock by coercivity and unblocking temperature properties. Geophysical Research Letters 17, 159–162.
Ma, Y.M., Yang, T.S., Yang, Z.Y., Zhang, S.H., Wu, H.C., Li, H.Y., Li, H.K., Chen, W.W., Zhang, J.H., Ding, J.K., 2014. Paleomagnetism and U-Pb zircon geochronology of Lower Cretaceous lava flows from the western Lhasa terrane: new constraints on the India-Asia collision process and intracontinental deformation within Asia. Journal of Geophysical Research - Solid Earth 119. http://dx.doi.org/10.1002/2014JB11362.
Mardia, K.V., Gadsden, R.J., 1977. A small circle of best fit for spherical data and areas of volcanism. Applied Statistics 26, 238–245.
McElhinny, M.W., 1964. Statistical significance of the fold test in palaeomagnetism. Geophysical Journal of the Royal Astronomical Society 8, 338–340.
McFadden, P.L., 1990. A new fold test for palaeomagnetic studies. Geophysical Journal International 103, 163–169.
McFadden, P.L., Reid, A.B., 1982. Analysis of paleomagnetic inclination data. Geophysical Journal of the Royal Astronomical Society 69, 307–319.
McFadden, P.L., Merrill, R.T., McElhinny, M.W., Lee, S., 1991. Reversals of the Earth's magnetic field and temporal variations of the dynamo families. Journal of Geophysical Research 96, 3923–3933.
Meng, J., Wang, C.S., Zhao, X.X., Coe, R., Li, Y.L., Finn, D., 2012. India–Asia collision was at 24°N and 50 Ma: palaeomagnetic proof from southernmost Asia. Science Reporter 2:925. http://dx.doi.org/10.1038/srep00925.
Metcalfe, I., 2009. Late Palaeozoic and Mesozoic tectonic and palaeogeographic evolution of SE Asia. Geological Society of London, Special Publication 315, 7–23.
Meyer, B., Tapponnier, P., Bourjot, L., Métivier, F., Gaudemer, Y., Peltzer, G., Guo, S.M., Chen, Z., 1998. Crustal thickening in Gansu-Qinghai, lithospheric mantle subduction, and oblique, strike-slip controlled growth of the Tibet plateau. Geophysical Journal International 135, 1–47.
Molnar, P., Stock, M., 2009. Slowing of India's convergence with Eurasia since 20 Ma and its implications for Tibetan mantle dynamics. Tectonics 28, TC3001. http://dx.doi.org/10.1029/2008TC002271.
Najman, Y., Appel, E., Boudagher-Fadel, M., Bown, P., Carter, A., Garzanti, E., Godin, L., Han, J., Liebke, U., Oliver, G., Parrish, R., Vezzoli, G., 2010. Timing of India-Asia collision: geological, biostratigraphic, and palaeomagentic constraints. Journal of Geophysical Research 115, B12416. http://dx.doi.org/10.1029/2010JB007673.
Orme, D.A., Carrapa, B., Kapp, P., 2014. Sedimentology, provenance and geochronology of the upper Cretaceous-lower Eocene western Xigaze forearc basin, southern Tibet. Basin Research http://dx.doi.org/10.1111/bre.12080.
Patzelt, A., Li, H.M., Wang, J.D., Appel, E., 1996. Palaeomagnetism of Cretaceous to Tertiary sediments from southern Tibet: evidence for the extent of the northern margin of India prior to the collision with Eurasia. Tectonophysics 259, 259–284.
Qiangba, Z.X., Xie, Y.W., Wu, Y.W., Xie, C.M., Li, Q.L., Qiu, J.Q., 2009. Zircon SIMS U–Pb dating and its significance of cumulate gabbro from Dengqen ophiolite, eastern Tibet, China. Geological Bulletin of China 28, 1253–1259 (in Chinese with English abstract).
Rowley, D.B., 1998. Minimum age of initiation of collision between India and Asia north of Everest based on the subsidence history of the Zhepure mountain section. Journal of Geology 106, 229–235.
Royden, L.H., Burchfiel, B.C., King, R.W., Wang, E.C., Chen, Z.L., Shen, F., Liu, Y.P., 1997. Surface deformation and lower crustal flow in eastern Tibet. Science 276, 788–790.
Searle, M.P., Windley, B.F., Coward, M.P., Cooper, D.J.W., Rex, A.J., Rex, D., Li, T.D., Xiao, X.C., Jan, M.Q., Thakur, V.C., 1987. The closing of Tethys and the tectonics of the Himalaya. Geological Society of America Bulletin 98 (6), 678–701.
Spurlin, M.S., Yin, A., Horton, B.K., Zhou, J., Wang, J., 2005. Structural evolution of the Yushu–Nangqian region and its relationship to syncollisional igneous activity, eastcentral Tibet. Geological Society of America Bulletin 117, 1293–1317.
Sun, Z.M., Jiang, W., Li, H.B., Pei, J.L., Zhu, Z.M., 2010. New paleomagnetic results of Paleocene volcanic rocks from the Lhasa Terrane: tectonic implications for the collision of India and Asia. Tectonophysics 490, 257–266.
Sun, Z.M., Pei, J.L., Li, H.B., Xu, W., Jiang, W., Zhu, Z.M., Wang, X.S., Yang, Z.Y., 2012. Palaeomagnetism of Late Cretaceous sediments from southern Tibet: evidence for the consistent palaeolatitudes of the southernmargin of Eurasia prior to the collision with India. Gondwana Research 21, 53–63.
Swanson-Hysell, N.L., Feinberg, J.M., Berquó, T.S., Maloof, A.C., 2011. Self-reversed magnetization held by martite in basalt flows from the 1.1–billion-year-old Keweenawan rift, Canada. Earth and Planetary Science Letters 305 (1):171–184. http://dx.doi.org/10.1016/j.epsl.2011.02.053.
Tan, X.D., Kodama, K.P., Chen, H., Fang, D., Sun, D., Li, Y., 2003. Paleomagnetism and magnetic anisotropy of Cretaceous red beds from the Tarim basin, northwest China: evidence for a rock magnetic cause of anomalously shallow paleomagnetic inclinations from central Asia. Journal of Geophysical Research 108 (B2):2107. http://dx.doi.org/10.1029/2001JB001608.
Tan, X.D., Gilder, S., Kodama, K.P., Jiang, W., Han, Y.L., Zhang, H., Xu, H.H., Zhou, D., 2010. New paleomagnetic results from the Lhasa Terrane: revised estimation of latitudinal shortening across Tibet and implications for dating the India–Asia collision. Earth and Planetary Science Letters 293, 396–404.
Tang, X.D., Huang, B.C., Yang, L.K., Yi, Z.Y., Qiao, Q.Q., Chen, L.W., 2013. Paleomagnetism and Ar-Ar geochronology of Cretaceous volcanic rocks in the middle Lhasa terrane, China and tectonic implications. Chinese Journal of Geophysics 56, 136–149 (in Chinese with English abstract).
Tapponnier, P., Peltzer, G., Le Dain, A.Y., Armijo, R., Cobbold, P., 1982. Propagating extrusion tectonics in Asia: new insights from simple experiments with plasticine. Geology 10, 611–616.
Tauxe, L., 2005. Inclination flattening and the geocentric axial dipole hypothesis. Earth and Planetary Science Letters 233, 247–261.
Tauxe, L., Kent, D.V., 2004. A simplified statistical model for the geomagnetic field and the detection of shallow bias in paleomagnetic inclinations: was the ancient magnetic field dipolar? In: Channell, J.E.T., et al. (Eds.), Timescales of the Internal Geomagnetic Field. Geophys. Monogr. Ser 145. AGU, Washington, D. C., pp. 101–115
Tong, Y.B., Yang, Z.Y., Gao, L., Wang, H., Zhang, X.D., An, C.Z., Xu, Y.C., Han, Z.R., 2015. Paleomagnetism of Upper Cretaceous red-beds from the eastern Qiangtang Terrane: clockwise rotations and latitudinal translation during the India-Asia collision. Journal of Asian Earth Sciences 114, 732–749.
Vand der Voo, R., 1990. The reliability of paleomagnetic data. Tectonophysics 184, 1–9.
Volkmer, J.E., Kapp, P., Guynn, J.H., Lai, Q.Z., 2007. Cretaceous-Tertiary structural evolution of the north central Lhasa Terrane, Tibet. Tectonics 26, TC6007. http://dx.doi.org/10.1029/2005TC001832.
Watson, G.S., Enkin, R.J., 1993. The fold test in paleomagnetism as a parameter estimation problem. Geophysical Research Letters 20, 2135–2137.
Yang, T.S., Ma, Y.M., Zhang, S.H., Bian, W.W., Yang, Z.Y., Wu, H.C., Li, H.Y., Chen, W.W., Ding, J.K., 2014. New insights into the India-Asia collision process from Cretaceous paleomagnetic and geochronologic results in the Lhasa terrane. Gondwana Research http://dx.doi.org/10.1016/j.gr.2014.06.010.
Yang, T.S., Ma, Y.M., Bian, W.W., Jin, J.J., Zhang, S.H., 2015. Paleomagnetic results from the Early Cretaceous Lakang Formation lavas: constraints on the Paleolatitude of the Tethyan Himalaya and the India-Asia collision. Earth and Planetary Science Letters 428, 120–133.
Yi, Z.Y., Huang, B.C., Chen, J.S., Chen, L.W., Wang, H.L., 2011. Paleomagnetism of early Paleogene marine sediments in southern Tibet, China: implications to onset of the India–Asia collision and size of Greater India. Earth and Planetary Science Letters 309, 153–165.
Yin, A., Harrison, T., 2000. Geologic evolution of the Himalayan–Tibetan orogen. Annual Review of Earth and Planetary Sciences 28, 211–280.
Yin, A., Dang, Y.Q., Zhang, M., McRivette, M.W., Burgess, W.P., Chen, X.H., 2007. Cenozoic tectonic evolution of Qaidam basin and its surrounding regions (part 2): wedge tectonics in the southern Qaidam basin and the Eastern Kunlun Range. Geological Society of America Special Papers 433, 369–390.
Zhu, D.C., Zhao, Z.D., Niu, Y.L., Dilek, Y., Mo, X.X., 2011. Lhasa Terrane in southern Tibet came from Australia. Geology 39, 727–730.
Zhu, D.C., Zhao, Z.D., Niu, Y.L., Dilek, Y., Hou, Z.Q., Mo, X.X., 2013. The origin and pre-Cenozoic evolution of the Tibetan Plateau. Gondwana Research 23, 1429–1454.
Zijderveld, J.D.A., 1967. A.C. demagnetization of rocks: analysis of results. In: Collinson, D.W., Creer, K.M., Runcorn, S.K. (Eds.), Methods in Palaeomagnetism. Elsevier, Amsterdam, pp. 254–286.